GLOBAL GPS TEC VARIABILITY DURING THE SOLAR MINIMUM 2008 PERIOD

A THESIS SUBMITED IN PARTIAL FULFILLMENT OF THE
REQUIREMENTS FOR THE DEGREE OF
MASTER OF SCIENCE IN PHYSICS
(SPACE PHYSICS)

ADDIS ABABA UNIVERSITY
SCHOOL OF GRADUATE STUDIES

MICHEAL ELIAS MUGORO
ADDIS ABABA, ETHIOPIA
July 2015

ADDIS ABABA UNIVERSITY
SCHOOL OF GRADUATE STUDIES
COLLEGE OF NATURAL SCIENCE
FACULTY OF CHEMICAL AND PHYSICAL SCIENCES
DEPARTMENT OF PHYSICS

The undersigned here by certify that they have read and recommend to the SCHOOL OF GRADUATE STUDIES for acceptance a thesis entitled "**GLOBAL GPS TEC VARIABILITY DURING THE SOLAR MINIMUM 2008 PERIOD**" by **MICHEAL ELIAS MUGORO** in partial fulfillment of the requirements for the degree of **MASTER OF SCIENCE IN PHYSICS(SPACE PHYSICS)**.

Dated: July 2015

Approved by the Examination Committee:

Advisor, Prof. Gizaw Mengistu Tsidu
(Bostwana International University of Science and Technology /Addis Ababa University)
_____

Examiner, _____ _____

ADDIS ABABA UNIVERSITY

Date: **July 2015**

Author: **MICHEAL ELIAS MUGORO**

Title: **GLOBAL GPS TEC VARIABILITY DURING THE SOLAR MINIMUM 2008 PERIOD**

Department: **DEPARTMENT OF PHYSICS**

Degree: **M.Sc.** Convocation: **June** Year: **2015**

Permission is herewith granted to ADDIS ABABA UNIVERSITY to circulate and to have copied for non-commercial purposes, at its discretion, the above title upon the request of individuals or institutions.

Signature of Author

Table of Contents

List of Figures

Abstract

The International GPS Service (IGS) Working Group on Ionosphere was created in 1998. Since then, the Scientific community behind IGS, in particular CODE, ESA, JPL and UPC, have been continuosly contributing to reliable IGS combined vertical total electron content (VTEC) maps in both rapid and final schedules. The total electron content (TEC) is a vital and most dominant ionospheric parameter that can cause Global Positioning System (GPS) signal delays, signal degradation and in extreme cases loss of lock. This results into inefficient operations of ground and space based Global Navigation Satellite System (GNSS) applications. The study of TEC variability is, therefore, useful for GNSS users in order to minimize errors where high levels of accuracy in measurements are required. This paper presents the results of the Global GPS total electron content (TEC) variation to better understand its typical periodic variability. The Global positioning System (GPS) TEC data was obtained from the International GPS Service (IGS) station with the highest data availability in the country and used to study the diurnal, seasonal, latitudinal and longitudinal variability for 2008. The strength and characteristics of the EIA were equally analyzed. In general, the diurnal variation of TEC shows a short- lived pre-dawn minimum, a steady early morning increase, followed by an afternoon maximum and gradual fall after sunset. The seasonal variability was greatest during the equinox, moderate during the Winter solstices and least during the Summer solstices. Latitudinal study of TEC shows the clear effect of EIA crest on the TEC variations in all the seasons. During this period of study, the so-called winter anomaly is seen near the equatorial and EIA crest region latitudes while it is found to be absent at low latitude outside the EIA crest. Evidences from our study show that the EIA was enhanced during the morning hours, suppressed during afternoon hours and a secondary enhancement was also noticed after sunset.

Acknowledgements

I give all the glory, honour and majesty to the Almighty God who made ways where there seemed to be no way. Thank you Jesus !

I deeply appreciate to my supervisor Prof. Gizaw Mengistu Tsidu for the strong academic supervision, guidance and intelligent suggestions he provided throughout the research period. He has not only been like a father but also a mentor and an inspiration to me. I am grateful to you for investing your time in me. Thank you so much.

I wish to thank the Addis Ababa University for providing the space, computer, internet resources and financial support. I also thank everyone at the AAU for being like family to me during this time. I also thank my colleagues and fellow students at the AAU, they all played a special part in being such good friends, and for interesting discussions especially during coffee breaks.

Special thanks to my mother, brothers, sister for the love, care, financial support and for being by my side all through my study time. May the almighty God bless you all.

Acronyms

TEC - Total Electron Content

GPS - Global Positioning System

GNSS - Global Navigation Satellite System

ROCSAT-1 - Republic of China satellite

IGS - International GPS servies

ESA - European Space Agency

JPL - NASA's Jet Propulsion Laboratory

UPC - Polytechnical University of Catalonia

NRCan - Energy Mines and Resources Canada

CODE - Center for Orbit Determination in Europe

EIA - Equatorial ionization anomaly

GIMs - Global Ionospheric Maps

SBAS - Space Based Augmentation Systems

TOPEX - TOPography EXperiment f-or Ocean Circulation

GBS - Brazilian Geodetic System

Low-Latitude Ionospheric Sensor Network - LISN

Red Argentina de Monitoreo Satellite continuo - RAMSAC

SBAS - Space Based Augmentation Systems

EGNOS - European Geostationary Navigation Overlay Service in Europe and Asia

WAS - Wide Area Augmentation Systemin USA

MSAS - Multi functional Satellite Augmentation System in Japan

GAGAN - GPS Aided Geo Augmented Navigation system in India

BGS - Bernese GPS Software

RINEX - Receiver Independent Exchange

IONEX - IONosphere Exchange

LOS - receiver line of sight

PPP - precise point positioning

MSLM - Mapping single layer model

BPE - Bernese Processing Engine

PCF - process control file

GPSEST - GPS Estimation

IPP - Ionospheric pierce point

Chapter 1

Introduction

Exploring the ionosphere is of utmost interest due to the the complexities associated with the region. Although, over the last century humanity has learned to use the properties of the ionosphere in tremendous ways, there are more to understand about the chemical and the physical of the region of the atmosphere. One of the parameters that can be used to study the ionosphere is the Total Electron content (TEC). It is an important descrptive quantity for the ionosphere. Also TEC is the integral of electron number density along the line of sight path from the satellite to the receiver and can vary dramatically [1]. Study of TEC variability over glob is useful to investigate the processes responsible for the ionospheric behavior over this region. TEC is significant in helping us to understand the short and long term changes of our upper atmosphere during major phenomena caused by factors like solar activities, geomagnetic storms and meteorological influences [2]. Among the various phenomena in the ionosphere, TEC is responsible for time delay which produces range errors in the GPS radio signal of a satellite to ground radio communication. At the same time, the perturbations in the GPS signals can be used as scientific information to investigate the ionospheric variability. These changes in the ionosphere affect navigation systems, surveillance systems and modern technologies such as communication systems since the signal from the satellite to the receiver must pass through the ionized layer [3]. As a consequence, a good description of the ionosphere is needed in order to improve the performance of the ionospheric models [3]. Hence it

is necessary to study the properties of the ionosphere such as its variability with respect to time of the day, season of the year, solar cycle, lunar tide effect, sudden stratospheric warming effect and magnetic storms effects. In this study however, sudden stratospheric warming effect and the magnetic storm effects on TEC will not be analyzed. Data used in this study were obtained from International GPS Service (IGS).

1.1 Aims and Objectives

This study will investigate the following variations of TEC:

1. The diurnal variability;
2. The day-to-day variability;
3. The monthly and seasonal variability; and
4. Latitudinal and longitudinal effect including equatorial ionization anomaly.

In this paper, we studied diurnal, monthly, seasonal and inter annual variation of equatorial ionization anomaly (EIA) in TEC with the help of GPS TEC IGS (International GPS Service) based measurement over glob. We have also studied longitudinal and latitudinal migration of EIA. The main purpose is to describe the behavior of the global ionosphere using global GPS TEC data during the solar minimum 2008 period.

1.2 Motivation

The computation of reliable global vertical total electron content of the Ionosphere (Vertical TEC or VTEC) is at the same time an useful and challenging goal. Useful because, in both Science and Technology fields, they can provide valuable information concerning space weather events, empirical model predictions, and user navigation improvement, among others (see for example [4, 3, 5]). Challenging because, at global scale, there are important parts of the Ionosphere which are not illuminated by any close Global Navigation Satellite

Systems (GNSS) satellite to receiver ray. This is due to the current lack of GNSS ground receivers, especially over the Oceans and in the Southern Hemisphere, among other regions. Moreover, the Inverse Problem to retrieve such VTEC maps from the Slant TEC (STEC) measurements is not straightforward. This is because these measurements do not directly provide the STEC (the carrier phases are affected by the ambiguity term, and the pseudoranges by the inter- frequency code bias, see for instance Hernndez-Pajares et al. [6]). In addition, conversion of VTEC is complicated by the variation of the electron content in space and time, with special difficulties close to the Equatorial Anomalies and during Ionospheric storms. The ionized particles in the ionosphere are produced mainly during the daytime through absorption of solar extreme ultraviolent (EUV) and X-ray radiation by the atmospheric neutral species. Largest fraction of the solar radiant energy is centered mainly at the equatorial and low latitude regions, hence many interesting phenomena are presented at these regions.

The ionospheric properties such as electron density, ion and electron temperatures, ionospheric composition, and dynamics vary with altitude, latitude, longitude, local time, season, solar cycle, as well as magnetic activity. Ionization changes at the equatorial and polar regions are known to be high compared to relatively moderate changes in the mid-latitude region. The variability of the equatorial and low latitude ionosphere is due to the large scale electrodynamics associated with the equatorial electrojet (EEJ), plasma fountain, equatorial ionization anomaly (EIA), equatorial wind, and temperature anomaly etc. The EEJ refers to an enhanced daytime eastward electric current in the E region due to a strong vertical polarization electric field developed in a latitude band of $\pm 3^{\circ}$ about the dip equator. This eastward electric field at the dip equator gets mapped onto F region through the ($E \times B$) drift, lifting the plasma to higher altitudes. The uplifted plasma diffuses down along magnetic field lines into both hemispheres creating two crests of plasma, one in each hemisphere (EIA generation). The overall process is called as the "fountain effect" [7]. The EIA can be described by a trough (minimum) in the ionization

densities around the dip equator and a crest (maximum) around $\pm 15^{\circ}$ magnetic latitude on each hemisphere. The EIA intensity on a day and its latitude of crest development explicitly depends on the EEJ strength at the equator. All these unique features at the equatorial and low latitude ionosphere are due to the perfect horizontal alignment of the geomagnetic field lines at the dip equator and the shifting between the geographic and geomagnetic equator[8].

1.3 Review on TEC

Many researchers have studied the morphological features of TEC at low and equatorial latitudes especially outside the African continent. Chauhan et al. [9] studied diurnal and seasonal variation of TEC at Agra in India and observed that the mean TEC varies from pre-dawn minimum to an afternoon maximum and then decreases. The low values were observed in winter, while high values were observed in equinox and summer months, and there was an absence of winter anomaly. Rama et al. [10] presented the temporal and spatial variations in TEC derived from the simultaneous and continuous measurements for the first time using the Indian GPS network of 18 receivers located from the equator to the northern crest of the equatorial ionization anomaly (EIA) region and beyond, covering a geomagnetic latitude range 10°- 24°N. In the analysis, they used 16 month data for the low sunspot activity period of March 2004 - June 2005. In their findings, along with the diurnal and seasonal variations in TEC, the day-to-day variability was also significant at all the stations, particularly during the daytime, with maximum variations at the EIA crest regions. Bagiya et al. [11] investigated diurnal and seasonal variations of TEC during low solar activity period (2005-2007) at Rajkot, a station near the equatorial ionization anomaly crest in India. It was found that TEC was maximum during equinoctial months (March, April, September and October) and minimum during winter months (November, December, January and February), with intermediate values during summer months (May, June, July and August). The temporal and spatial variation at the equatorial

and low latitude regions are significant compared to mid latitude regions owing to its dynamic nature due to well known phenomenon equatorial ionization anomaly (EIA) associated with it and is a challenging problem even today to model it [12, 13, 14]. The equatorial ionospheric anomaly (EIA) is characterized, in terms of latitudinal distribution of ionization, showing a trough at the magnetic equator and crests at about $\pm 17^{\circ}$ magnetic latitude [7]. Many theories, like the diffusion theory [15, 16] and the electrodynamic drift theory [17, 18, 19, 20] have been known to explain the anomaly crest. Although Mitra, [15] suggested role of diffusion, but correct explanation was given after Martyns electromagnetic drift theory (upward plasma drift followed by diffusion). The fountain effect and associated anomaly can cover more than 30°latitudes on either side of the magnetic equator. The perseverance of the EIA into the nighttime hours depending on the season and solar activity is known to be produced by the post- sunset enhancement in the eastward electric field produced by the F-region dynamo action. This dynamo action, in turn, results from the eastward component of the thermospheric wind blowing in the region of the decreasing dawn-to-dusk E-layer Pedersen conductivity distribution [21]. Balan and Bailey, [22] further studied the plasma fountain including neutral wind also and shown that the plasma velocity turning more poleward in that hemisphere, where the wind is pole-ward.

The formation of the EIA is seen in the total electron content (TEC), which is the integral of electron number density along the line of sight from satellite to receiver and can vary dramatically from day to day [23, 1, 11, 14]. The latitudinal variation of daily TEC was found to correlate with strength of the electrojet current [1, 10]. On the other hand long-term averages of TEC do have seasonal variations. The strength of monthly anomaly crest increases with solar activity and shows a winter anomaly with the winter strength larger than the summer strength for all solar activity levels [23]. The strength of equatorial anomaly shows semiannual variations. In the Indian sector, the diurnal variation in TEC was reported by Rama et al., [10] who showed that at EIA crest, day maximum in TEC

occurs between 13:00 and 16:00 LT and a short lived day minimum occurs between 05:00 to 06:00 LT. He further showed that in the Indian sector the EIA crest is found to occur in the latitude zone of 15° to 25° N geographic latitudes. All these studies have shown the characteristic features of the TEC for the Indian region.

1.4 Final Remarks

Most of the literatures reviews suggests many important mechanisms and results which are consistent in our study. However their argument did not take account of the whole global region which is the focus of our study. Using GPS-TEC-IGS from most of the receivers over glob, we intend to provide observational evidence that clearly demonstrates how the ionization phenomena at the EIA and generally over glob is affected by season, by each month of the year and by day-to-day variability during the solar minimum 2008 period and how these TEC variability could affect the behavior of the EIA, taking into consideration the aforementioned mechanisms.

Chapter 2

THE EARTH ATMOSPHERE AND THE IONOSPHERE

2.1 Earth's Atmosphere

The envelop of gases surrounding the earth, which is a stable mixture of several types of gases from different origins is known as the atmosphere. It is kept in space by gravitational attractions. Nitrogen and Oxygen make up to 99% of the atmosphere at sea level, with the remainder comprising CO_2 , noble gases and traces of many gaseous substances. Based on the temperature changes with height, the Earth's atmosphere can be divided into mainly four distinct regions: troposphere, stratosphere, mesosphere and thermosphere. The ionosphere is bounded in the region of thermosphere, and it is a layer under investigation in the research work and shall be discussed in more detail (see Figure 2.1).

2.2 Layers of the Atmosphere

Troposphere is the lowest part of the atmosphere and extends to the altitude of 8 km above the poles and 18 km over the equator. The temperature generally decreases with height in the troposphere. The troposphere contains 99% water vapor in the atmosphere which plays a major role in regulating air temperature because it absorbs solar energy and thermal radiation from the planet's surface. The layer is bounded at the top by the

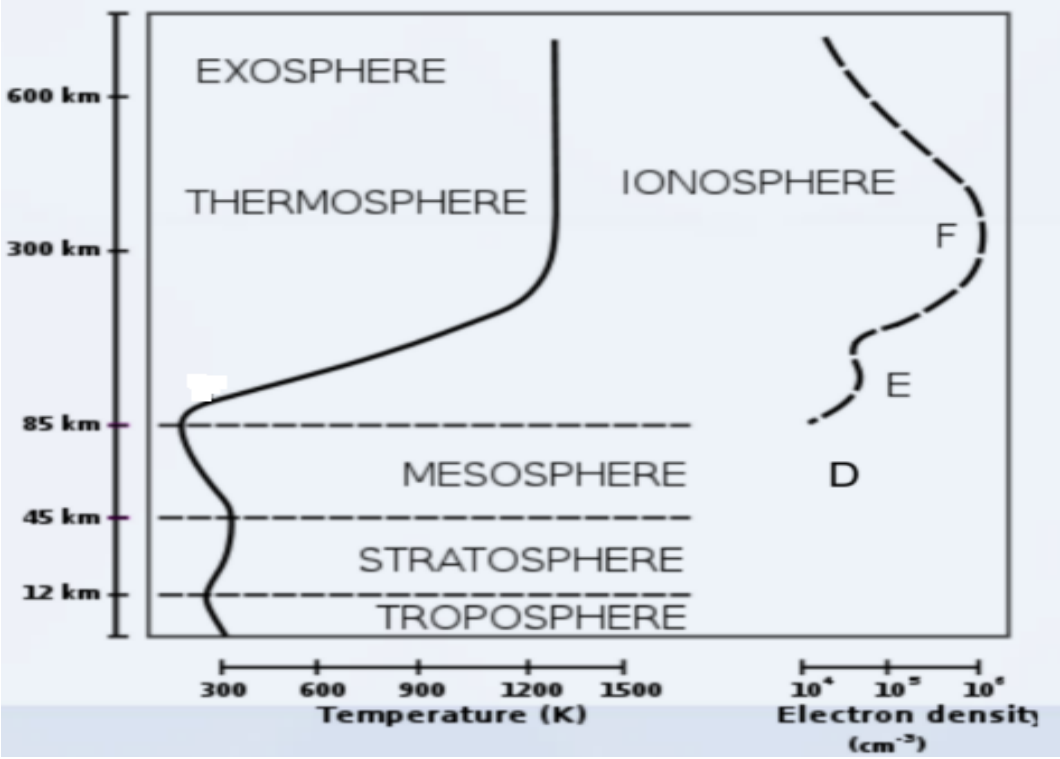

Figure 2.1: Relationship of the atmosphere and ionosphere (Source: Wikipidia.)

tropopause [24].

Stratosphere is also an important layer to this research work because this is where the SSW is initiated. It is the second layer of the earth's atmosphere, and it starts at an altitude of 8 km - 18 km and extends up to 50 km. It is so named because the stratified layers within it have a temperature profile that increases with altitude [25]. The stratosphere holds the ozone that absorbs harmful UV radiation and prevents it from reaching the earth's surface. Every winter the stratosphere over the pole at the winter hemisphere cools, this begins when the sunlight can no longer provide the energy to heat the ozone. Without this energy, the stratosphere cools rapidly, creating a thermal imbalance with the warmer stratosphere further south. This imbalance creates a large pressure difference and combined with the Coriolis effect, creates a large strong jet stream, spring the globe in the stratosphere in the eastwards direction (this is most famous in the Antarctica and Arctic region due to extremely low temperature in this region). This

system is known as the polar night jet, and a strong vortex known as the polar vortex is contained within it. The polar vortex increases and decreases in strength depending upon how cold the polar stratospheric atmosphere becomes during winter. The colder the polar stratosphere becomes, the stronger the polar vortex - and vice versa. This action leads to generation of ozone hole and the consequent split of the polar vortex company by a rise in stratospheric temperature. This event is referred to as SSW. The stratospheric layer is bounded at the top by the stratopause.

Mesosphere is a layer that extend from 50 to 80 km and characterized by decrease in temperature with increasing altitude. The region is considered to be the coldest of Earth atmosphere reaching a minimum of 180 K at 80 km altitude. The chemical compositions are fairly uniform and pressures are very low. The layer is bounded at the top by the mesopause.and

Thermosphere is a region of high temperature and density is very low. The thermosphere include the ionosphere and extend out to several hundred kilometers. The temperature increase is due to the absorption of intense solar radiation by the limited amount of molecular oxygen present. The thermopause is the level at which the temperature stops rising with height which depend on the solar activity.

2.3 Ionosphere

The ionospheric region is the shell of electrons consisting of electrically charged atoms and molecules which surround the Earth, and extends from a height of about 50 to 1000 km [26]. The main distinction between the ionospheric region and other regions of the atmosphere is that the former contains more charged particles[27]. The formation of the ionosphere depends on the activities of the Sun, because the solar extreme ultraviolet (EUV) light and X-ray radiation from the Sun are the main sources of plasma and energy for the ionosphere. The process by which the EUV light and X-ray radiation from the

Sun interact with neutral atoms giving rise to free electrons is called photoionization. Because of this process, the ionosphere consists of free electrons and ions.The net value of the number of free ions and electrons in the ionosphere is determined by the rate at which specific species of ions combine with electrons to form neutral atoms. This process is known as recombination and it occurs in two stages[26]:

Radiation recombination is the process whereby electrons combine directly with positively charged ions, converting them into neutral atoms and emitting a photon to conserve energy and momentum

$$O^+ + e^- \longrightarrow O + photon \tag{2.3.1}$$

The dissociative recombination process occurs in two stages:

In the first stage the positive ions (eg N^+) which formed during the photoionization process interact with a neutral atom forming a positively charged molecular ion:

$$N^+ + O_2 \longrightarrow NO^+ + O \tag{2.3.2}$$

In the second stage the electrons combine again with a positively charged ion (NO^+) to produce two neutral atoms:

$$NO^+ + e^- \longrightarrow N + O \tag{2.3.3}$$

Dissociative recombination is a faster mechanism than radiative recombination to loose electrons from the ionosphere. During sunset, the recombination process ceases, which results in a gradual drop in electron density as night progresses. Electron density is at its greatest during the middle of the day when photoionization is high. Because different gas atoms and molecules are more abundant in some regions of the neutral atmosphere than others, ionization and recombination of different species result in a different electron density distribution within different layers of the ionosphere. These layers are called D,

E, F_1 and F_2 and are discussed in the next section.

2.4 Ionospheric Layers

2.4.1 D-Layer

The D-layer is the lowest layer and lies between 50 and 90 km above the surface of the Earth. It is ionized during the day (mostly at noon) and quickly deionizes at night. The ionization is caused by solar X-ray radiation or Lyman alpha-hydrogen from the Sun at wavelengths of 1 to 10 $\mathring{A}$. This lower layer absorbs the lower frequencies (below 10MHz) and allows the higher frequencies to pass to outer layers. The D-layer plays a less significant role in ionospheric tomography, because it shows much lower electron density than the F-layer and it has a negligible contribution to the total electron content (TEC) within the ionosphere. It is only present during the day, reducing and disappearing as the Sun sets. It may, however, sometimes remain due to the ionization effect of galactic cosmic rays [28]. At the lower level of this layer, the density of electrons is very high and the recombination of ionized particles occurs rapidly. The D-layer quickly reaches full ionization when the Sun is up and immediately loses its energy after the Sun goes down. It is important for radio propagation because:

it absorbs energy from waves at Maximum Frequency (MF), High Frequency (HF) and Very High Frequency (VHF), and

it reflects Low Frequency (LF) and Very Low Frequency (VLF) waves.

2.4.2 E-Layer

The E-layer lies above the D-layer and is found between about 90 and 120 km above the surface of the Earth. It is ionized by soft X-rays of wavelengths ranging from 10 to 100 $\mathring{A}$. Like the D-layer, the E-layer is ionized during the day and the ionization process does not last long. The photoionization and recombination processes occur more slowly in the

E-layer than in the D-layer. The former plays an important role in the quality of radio communication and radio waves, in that it refracts HF waves that would penetrate the D-layer. According to Giraud and Petit [29] the E-layer corresponds to a moderately dense (10^3 to 10^5 cm^3) layer of molecular ions $NO^+ and O_{2+}$ in the midst of thin atomic layers called the Sporadic E (E_s) phenomenon. The charged particles in the E-layer are the results of ionization of molecular Oxygen (O_2) generated by soft X-rays as well as EUV radiation (1-10 nm) [28]. Therefore the E-layer can reflect radio waves with frequencies lower than about 10 MHz. At night this layer begins to disappear because the primary source of ionization is no longer present.

2.4.3 F-Layer

The F layer is divided into two layers which is $F_1 and F_2$ layer:

F_1**-Layer** is situated below the F_2 layer and lies between 150 and 200 km above the surface of the Earth. The ionization of atoms such as Oxygen (O_2) and Nitrogen (N_2) occurs by Lyman Continuum or He emission and disappears after sunset. During the night the F1-layer quickly loses its ionization and disappears. Acoording to Giraud and Petit [29], the F_2 layer is where the peak of O^+ ions occurs while the transition between molecular and atomic ions takes place in the F1-layer. There are certain conditions where by the F1-layer is not present at all [30]. In particular, this layer is never present at night. It is rarely found in winter but is likely to appear during daytime in summer when the solar zenith angle is small and hence the peak altitude of ionization is lower [31]. The F_2-layer is likely to appear during solar minimum periods when the rate of ionization is low and the transition altitude between molecular and atomic ions is higher.

F_2**-Layer** lies between about 250 and 400 km, and is the uppermost layer of the bottomside ionosphere. Ionization in this layer occurs due to the photoionization of atomic oxygen by extreme EUV solar radiation from the Sun. This layer is very thick, more active and more highly ionized, but its ionization decreases during and after sunset. Since F_2 layer is

the highest layer of the ionosphere, it consists of a greater concentration of free electrons and ions. It is the most important layer for HF radio propagation because:

1. It is the only layer that survives at night and is present 24 hrs of the day.
2. It reflects the radio waves needed for high frequency communication and broadcasting.
3. Its high altitude allows the longest distance and communication paths.

Further details on the ionospheric layers can be found in [26]; [32]. The variation of the ionospheric electron density with altitude is dependent on the different molecules that are dominant in a specific range of altitudes. Because the neutral gas density decreases with height, there are fewer neutral atoms allowed to participate in the ionization process at higher altitudes. The radiation intensity also increases at a lower altitude. Since the ionization appears differently at different ionospheric levels, it produces layers or regions which may be identified by their interaction with radio waves.

2.5 Geographic Regions of the Ionosphere

There are three major regions of the global ionosphere. These are the high-latitude, mid- latitude and equatorial regions. In this section, I will briefly describe the main characteristics of the individual regions (see Fig. 2.2).

2.5.1 Low and equatorial latitudes

The larger fraction of solar energy is absorbed within $\pm 30^{\circ}$ latitude zone centered on the equator [33], so it is expected to have larger ionization at the region. However, one of the most prominent features in the ionosphere, known as equatorial anomaly (also called the Appleton Anomaly), occurs at the low latitudes, given origin to a depletion at equatorial latitudes and two ionizations crest at low latitudes as explained below. The electric field

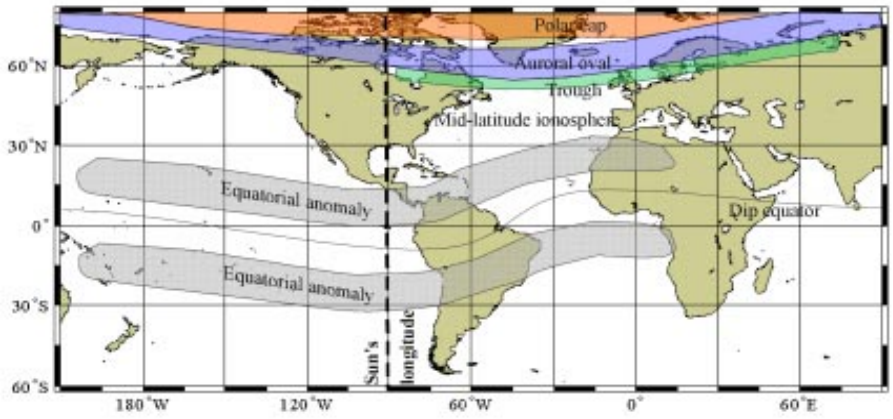

Figure 2.2: Major geographic regions of the ionosphere (Source: after Bishop et al. (1991)).

configuration, which is eastward during the day, produces an upward drift ($E \times B$) drift leading to a plasma fountain. The lifted plasma by the fountain effect then diffuses downward along the geomagnetic field lines due to the gravitational force and pressure gradient, which result in the ionization enhancement on both sides of the magnetic equator at $\pm 15^{\circ}$ latitude. The low latitude anomaly may exhibits asymmetry behavior between

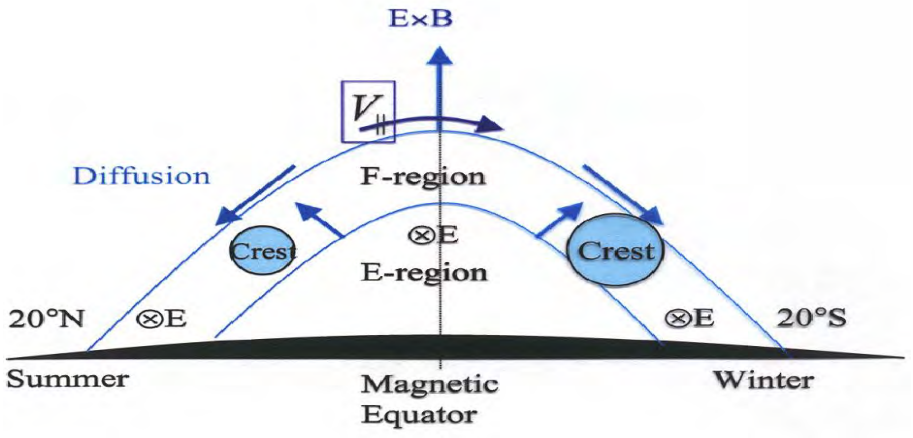

Figure 2.3: Fountain effects and asymmetry of the equatorial anomaly. An interhemispheric wind blowing from the summer to the winter hemisphere produces an asymmetry between two peak densities of the equatorial anomaly. E denotes an eastward electric field, and B is the northward geomagnetic field. Scheme Anderson and Roble (1981).

the northern and southern ionization crests due to an inter hemispheric wind blowing

from the summer to winter hemisphere. The behavior is represented in the Fig. 2.3. In the summer hemisphere, plasma moves upward along the geomagnetic field lines, while plasma moves downward in the winter hemisphere. Therefore the plasma is transported from the summer hemisphere to the winter hemisphere. As result, the equatorial anomaly crests in the winter hemisphere are generally larger than in the summer hemisphere Fig. 2.3.

2.5.2 Middle latitude ionosphere

The middle latitude ionosphere is a relatively less variable and disturbed region and as a result of this, most of the ionosphere sensing instruments, observations and measurements are best obtained at this region. This latitude is also usually free of the effects imposed by the horizontal magnetic field geometry associated by the equatorial region. The ionospheric plasma is constrained to move along the geomagnetic filed lines Fig. 2.4 hence the thermospheric neutral wind effectively transport plasma along the field lines into higher and lower altitudes regions in which recombination rates are different resulting in changes of the plasma density. The poleward neutral wind move plasma down to lower altitude where recombination rate is large during the day. As a result, the peak height of F_2 is reduced and there is a decrease in the peak electron density but during the night the typically equatorward wind move plasma up. Therefore the recombination of the plasma with neutrals decreases, the peak height increases and the night time peak electron density is partially maintained.

2.5.3 High-Latitude Region

In addition to photonionization, collisional ionization is another source of ionization in the high-latitude region. The main reason for this is the fact that the geomagnetic field lines are nearly vertical in this region leading to the charged particles descending to E layer altitudes (about 100 km). These particles can collide with the neutral atmospheric

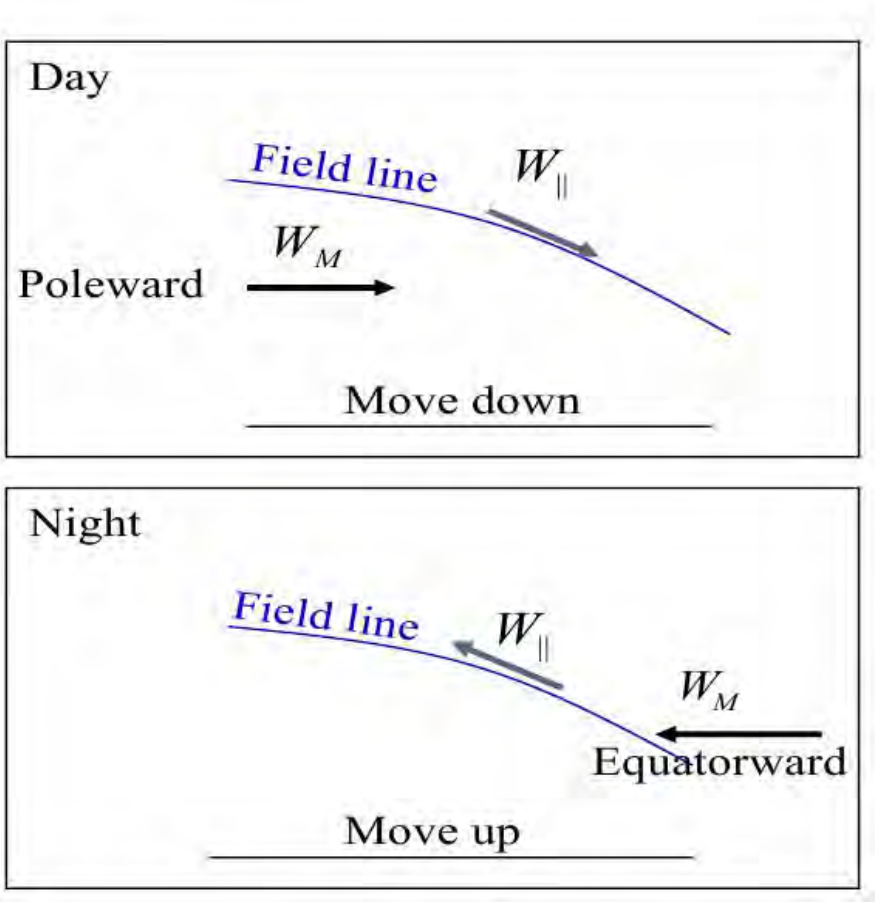

Figure 2.4: Vertical plasma drifts due to the meridional neutral wind (W_M). $W_{||}$ is the meridional wind component along the geomagnetic field line (Source: Ja Soon Shim 2009).

gases causing local enhancements in the electron concentration, a phenomenon which is associated with auroral activity. Auroral activity can also be regarded as an interaction between magnetosphere, ionosphere, and atmosphere. The auroral zones are relatively narrow rings situated between the northern and southern geomagnetic latitudes of about 64° and 70°. In general, the intensity and the positions of the auroral ovals are related to geomagnetic disturbances. The ovals expend towards the equator with increasing levels of geomagnetic disturbance [26]. On the equatorial side of the auroral ovals lies the mid-latitude trough which is a narrow region of the ionosphere with a width of a few degrees. It can be characterized by a sudden drop in the critical frequencies and electron densities by a factor of two or more. This occurs essentially at night time primarily due to the

increased recombination as a consequence of the shorter high latitude day time ionization periods[34]. The direct interaction between the magnetosphere and the interplanetary magnetic field results in the dayside cusp or cleft. It is typically 2° to 4° wide and located at 23° the geomagnetic latitude of 78° to 80° near local noon. The phenomenon can be characterized with enhancements in electron densities at all altitudes. The geographical regions enclosed by the auroral rings are called the polar caps. Our understanding of the polar cap region is rather limited due to the lack of available information. The polar caps are largely affected by solar flares and mass ejections from coronal holes (relatively cool open structures of the solar corona) causing D region electron density enhancements.

2.6 E Region and F Region Dynamo

The ionosphere acts not only as the reflection or absorption layer of the radio wave, but also as an electric current layer. Low latitude electric fields, plasma drifts and ionospheric currents result largely from the dynamo action of E and F neutral winds, but can be significantly perturbed by lower atmospheric gravity and planetary waves during magnetically quiet times [[35, 33]]. The E layer dynamo electric field mapped along the highly conducting magnetic field lines controls the plasma dynamic/transport of the equatorial F- region during the day, whereas the F dynamo electric field can develop only during the night as result of the disappearance of E layer conductivity after sunset.

2.6.1 E Region Dynamo

The electric fields are generated in the E region by ionospheric dynamo driven by atmospheric tidal winds [36]. The winds, which are established by the absorption of solar radiation in the stratosphere and troposphere, affect the movement of charged particles. Ions and electrons assumes a cyclotron movement in the present of the magnetic field ($\overrightarrow{B}$). The

interaction between the tidal wind (U) and $\overrightarrow{B}$ gives rise to a relative movement between the ions and electrons which leads to an induced electric field as a result of $\overrightarrow{U}X\overrightarrow{B}$. The induced current associated with this is not stationary, i.e. $\overrightarrow{\nabla}.\overrightarrow{J} \neq 0$. This makes electric field polarization ($\overrightarrow{E}_p$) to be established in the E region without any current divergent. The total electric field in this ionospheric region:

$$\overrightarrow{E} = \overrightarrow{E}_P + (\overrightarrow{U}X\overrightarrow{B}), \tag{2.6.1}$$

and the total current flowing in the same direction of the field can written as:

$$\overrightarrow{J} = \sigma.\overrightarrow{E} \tag{2.6.2}$$

where σ is the electrical conductivity tensor. Substituting equation (2.6.1) in (2.6.2) we have:

$$\overrightarrow{J} = \sigma.(\overrightarrow{E}_P + (\overrightarrow{U}X\overrightarrow{B})) \tag{2.6.3}$$

The current flowing in a conductor, which in this case is the E region, is not divergent, then the divergent of equation 6.3 gives:

$$\overrightarrow{\nabla}.\overrightarrow{J} = \overrightarrow{\nabla}.(\sigma.(\overrightarrow{E}_P + (\overrightarrow{U}X\overrightarrow{B})) = 0 \tag{2.6.4}$$

According to Kelley, [37], the physics of the dynamo region can be understood by considering it as a conductive thin plate subjected to a constant zonal electric field ($\overrightarrow{E}_X$), perpendicular to $\overrightarrow{B}$ as shown in Fig. 2.5. The B and the electric field in the region are perpendicular to each other. There are essentially two types of current in the equatorial E region, which are the Hall and Pederson current. The Hall current ($\sigma_H E_X$) flows in the direction perpendicular to both electric field (E_X) and the $\overrightarrow{B}$, while the Pederson current ($\sigma_H E_P$) flows parallel to the electric field ($\overrightarrow{E}_X$) and perpendicular to $\overrightarrow{B}$. The Hall current cannot flow across the boundary and this leads to accumulation of charges at both boundary. These accumulated charges gives rise to upward electric field polarization ($E_Z a_Z$). In response to this polarization, the Hall current ($\sigma_H E_X$) and the Pederson

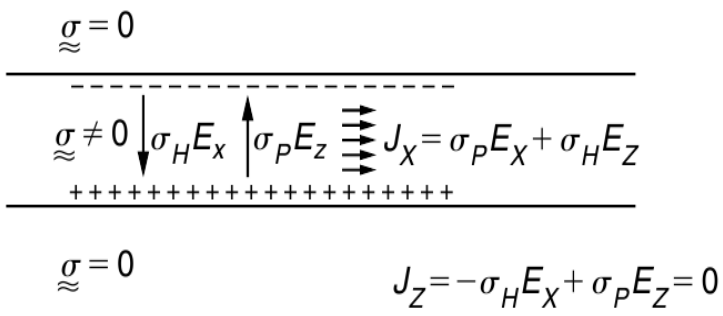

Figure 2.5: E region electrodynamics. (Source: Kelley (2009)).

current (($\sigma_P E_Z$)) are in steady state but no vertical current can flow hence both Pederson and Hall current cancels. This gives:

$$\sigma_H E_X = \sigma_P E_Z \tag{2.6.5}$$

Dividing both side by σ_P :

$$E_Z = (\frac{\sigma_H}{\sigma_P}) E_X \tag{2.6.6}$$

In the horizontal direction the current add up and then form an intensified field called equatorial electrojet:

$$J_X = \sigma_H E_Z + \sigma_P E_X \tag{2.6.7}$$

Substituting equation (2.6.6) in (2.6.7) we have:

$$J_X = [\frac{\sigma_H^2}{\sigma_P^2} + 1]\sigma_P E_X = \sigma_C E_X \tag{2.6.8}$$

where σ_C is called Cowling conductivity. The equatorial electrojet is determined by tidal winds that create the global component of the daily zonal electric field measured at the equator. It is the strong current around $\pm 3^\circ$ latitude of the geomagnetic equator.

2.6.2 F Region Dynamo

While the E layer dynamo electric fields are generated by winds associated with the tidal waves arising from solar ultraviolet radiation (UV) absorption in the ozone layer and

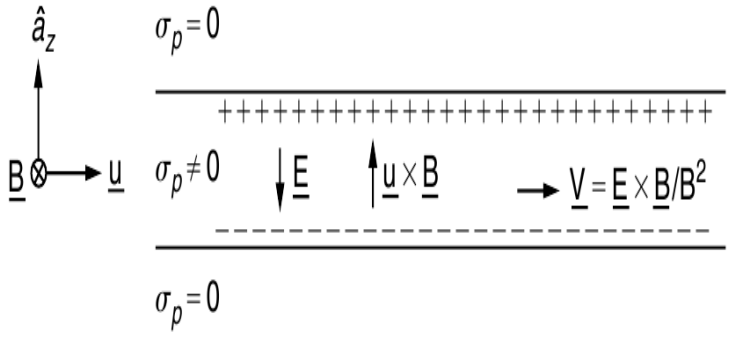

Figure 2.6: F region electrodynamics. (Source: Kelley (2009)).

atmospheric water vapor, as well as from lunar gravitational field, the thermospheric winds that are responsible for the F layer dynamo electric fields results from solar thermal tides arising from the solar extreme ultraviolet radiation (EUV) absorption in the thermosphere [33]. Fig. 2.6 illustrates the electrodynamics of F region as a narrow conducting thin layer. σ_P is constant inside the layer and zero elsewhere and zonal wind U is constant everywhere. The thermospheric winds cause induced motion of charged particles in the direction of $(\overrightarrow{U} X \overrightarrow{B})$. The movement perpendicular towards both B and the wind itself, gives rise to an electric field which tend to establish a polarization field as a result of accumulated charges at the two boundaries as shown in Fig. 2.6. During the day conductivity is large in the E-region and there is high mobility across magnetic field lines, which behave as good conductors, and then the electric field polarization is discharged by current flowing along magnetic field line through the E region and thus close the circuit between the E and F layer. During night hours when conductivity of E decreases drastically, the circuit is not closed, this give rise to electric field polarization resulting in the movement of plasma along the magnetic field lines [[30, 36]]. The drift velocity of the motion can be represented by the equation:

$$\overrightarrow{V} = (\frac{\overrightarrow{E} X \overrightarrow{B}}{B^2}) \tag{2.6.9}$$

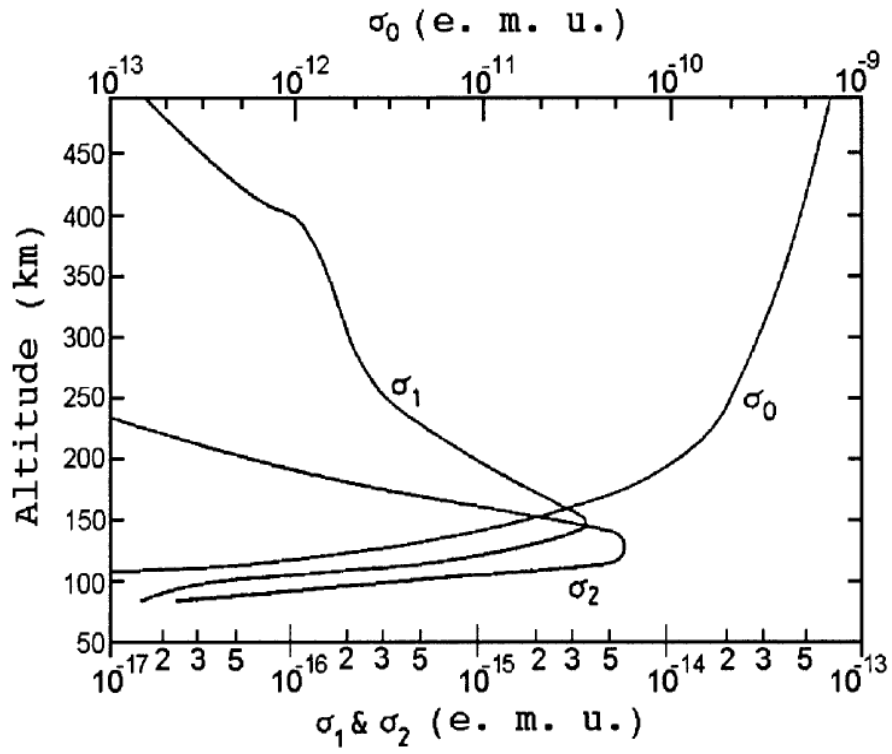

Figure 2.7: Vertical profile of the Parallel (σ_0), Pederson(σ_1) and Hall (σ_2) conductivities. (Source: Abdu (2005))

2.7 Altitude Variation of Conductivity

The ionosphere conductivity is due to the drift motion of the electron ($E \times B$ drift) and presents its maximum in the E region where only electron practically drifts to the direction of $E \times B$. The conductivity depends on various parameters such as location, time, season and solar activity. There are three types of conductivity: Parallel conductivity which is usually in the direction parallel to the magnetic field line and denoted as "σ_0 ", Pedersen conductivity which is usually in the direction perpendicular to the magnetic field and parallel to the electric field it is denoted as "σ_1 ", and Hall conductivity in the direction perpendicular to both the magnetic and electric fields. It is denoted as "σ_2 ". The vertical profiles of these conductivities are presented in Fig. 2.7. Fig 2.7 also shows Pederson conductivity peak at around 140 km and the Hall conductivity peak at around 120 km. Their values decreases rapidly above and below these heights [33].

The conductivity parallel to the magnetic field increases strongly with altitude due to decreasing collisions with the neutral gas. The parallel conductivity is always much higher than the conductivity perpendicular to the magnetic field. The movement of a class of charged particles perpendicular to the magnetic fields depends on the ratio of the collision frequency (ν) to the gyrofrequency (ω_g). If $\nu \gg \omega_g$ then collisions prevent the particle from gyrating and the particles move in the direction of the electric field, as a Pedersen current. If, on the other hand, $\nu \ll \omega_g$ then the particles predominantly drift perpendicular to the electric field.

2.8 Factors Affecting the EIA

The EIA development depends on a complex coupling of a number of atmospheric processes but for most it is dependent on winds in the upper atmosphere. Two different processes, the E and F region dynamos control the EIA formation during the day and its evolution during the night. The EIA shows considerable variability with local time, longitude and season. A description of a few factors creating variability in the EIA will be presented next.

2.8.1 Magnetic Equator

The direction of the Earths magnetic field can be given in terms of magnetic inclination and declination. The magnetic or the DIP equator are the latitudes where the inclination or dip is zero. The magnetic equator does not follow the geographic equator. Its alignment from the geographic equator varies considerably with longitude but neutral atmospheric winds are generally aligned with the geographic equator. At longitudes where the magnetic equator lies far off from the geographic equator, an asymmetry in the equatorial arcs is expected due to variations of the neutral winds with latitude. In Fig. 2.8 [38], the Sun is aligned with the magnetic equator and the neutral winds are assumed to blow symmetrically on to both sides of the DIP equator. As the Earth rotates, the

magnetic dipole shifts with respect to the Sun and the sub solar point lies entirely to the north of the DIP equator even during equinox conditions [38]. This resulting asymmetry partially explains the longitudinal variability in the structure of the equatorial arcs.

2.8.2 F-region Neutral Winds

The north and south peaks of the EIA have asymmetries during summer or winter solstice due to the nature of the resulting meridional neutral winds in the F-region. The winds blow away from the sub solar point which is generally located north or south of the EIA. During solstice, winds from the sub solar point tend to push the plasma into the winter hemisphere and the anomaly is more developed on to one side of the magnetic equator. Thus, a seasonal shift in the sub solar point accounts for some of the asymmetric seasonal variability in the EIA. This same process is responsible for a shifting of the latitude at which the peak density in the EIA occurs. At a certain altitude the diffusion of the plasma down and along flux tubes in the equatorial fountain can be balanced against the neutral north or south winds, the plasma tends to lie suspended if the wind is against the downward drift. This piling of plasma will eventually be where we see the peaks of the EIA occur thus moving the arc closer to the geomagnetic equator. Another complex F-region process called the pre-reversal enhancement is known to be responsible for a sudden increase in the vertical plasma drift in the F-region, and hence a impulsive enhancement in the EIA is predicted to occur in the evening local time sectors due to this sudden upward motion.

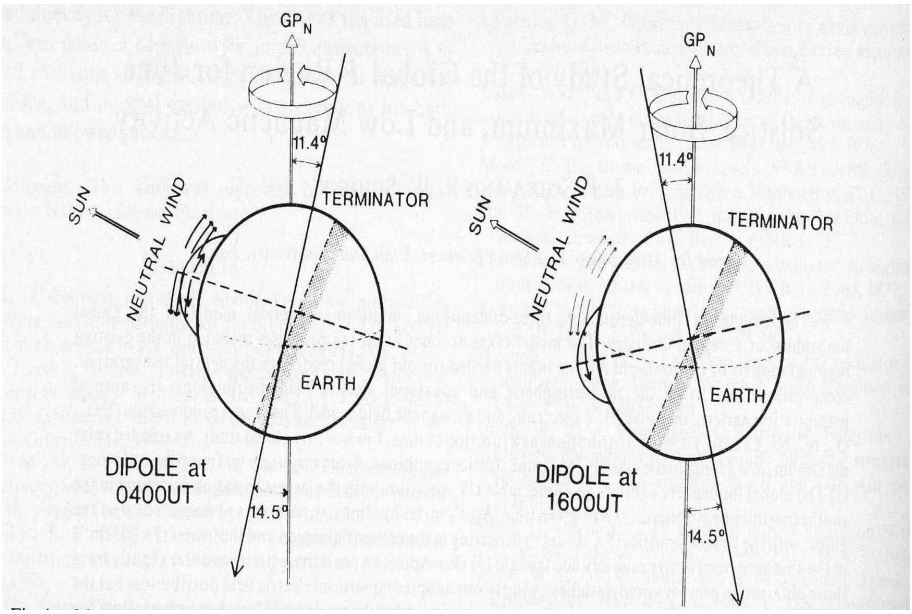

Figure 2.8: F-region meridional winds, (Source: Shankar (2007)).

Chapter 3

Data description and method of analysis

3.1 Data description

3.1.1 IGS (International GPS Service) TEC data

IGS (International GPS Service) provides the highest precision of GPS satellite orbits, and precise positions (5 mm) for 350 worldwide reference stations [39]. Usually, the single ionospheric layer assumption is considered to convert the slant path TEC to vertical TEC with a mapping function. Currently, five analysis centers routinely provide GIMs (global ionopheric maps) of vertical TEC using the growing global network of dual-frequency GNSS receivers [39]. These are CODE [40], JPL [41], European Space Agency(ESA) [42], Polytechnical University of Catalonia(UPC) [43] and the Energy Mines and Resources Canada(NRCan)[44]. The used global IGS TEC data have a time resolution of 2 hr and a grid spacing of 5×2.5 in longitude and latitude,respectively, with errors of several TEC Units ($TECU, 1TECU = 10^{16} el/m^2$) [43]. The errors of the GIM/CODE are determined by comparing with an independent source of TEC. The reference TEC values are provided by dual frequency altimeters on board of TOPEX, JASON, and ENVISAT satellites. Because the altimeters are working over oceans, this comparison is considered as a pessimistic determination of the global TEC map actual errors. The original global TEC data were arrayed in terms of the coordinate system of geographical latitude (from

-87.5° to 87.5° at each 2.5°) and longitude (from -180° to 180° at each 5°). The TEC measurements made by the widely distributed network of ground-based GPS receivers are incorporated into the data product. Data gaps, such as those over the oceans where the GPS occultations are not available, are filled in through interpolations and data assimilation techniques [45]. These products are finally validated against the TOPEX TEC data. The IGS TEC maps have been recognized and extensively used for studying the properties and variations of the ionosphere [[46, 43]]. The global IGS TEC maps are used in the present study to identify the day-to-day variations in the ionosphere. Because the UFK waves are trapped in the equatorial region, their effects on the ionosphere are expected to be seen at low latitudes near 15 °- 20 °. It is known, however, that the neutral wind and electric field effects on the ionosphere are dependent on the geomagnetic field configuration as the electrons are constrained to the magnetic field lines. That is why the distribution of the ionospheric parameters, including TEC as well, is usually presented in geomagnetic latitude instead of geographic one. Early investigations [47] demonstrated the benefit of using the modified dip (modip) latitude, introduced by [47] to describe the variability of the densest part of the ionosphere, particularly at mid and low latitudes. The modip latitude which is adapted to the real magnetic field, example, to the magnetic inclination (dip), is defined by: $tan\mu = I/\sqrt{cos\phi}$, where μ is modip latitude, I is the true magnetic dip (usually at a height of 350 km), and ϕ is the geographic latitude. Modip equator is the locus of points where the magnetic dip (or inclination) is 0. In the equatorial zone, the lines of constant modip are practically identical to those of the magnetic inclination, but as latitude increases, they deviate and come nearer to those of constant geographical latitude. The poles are identical to the geographic ones [48]. Then for the purpose of this study, the global TEC data were rearrayed in terms of the coordinate system of modip latitude, from -80° to 80° at each 5°, and geographic longitude, from -180° to 180° at each 15°. The TEC data falling into the area 5° (modip latitude) × 15° (longitude) were averaged.

3.2 Method of analysis

3.2.1 TEC measurement and Instrumentation

Many measuring instruments have been used to measured TEC value for decades. For example the Faraday rotation, Ionosonde and the Incoherent Radar systems located close to the magnetic equator in Peru. However, nowadays TEC measurements are often made using GNSS data because of the improved global coverage of the GNSS observation network. Ionospheric TEC has been widely studied using GNSS observations in recent years [11] and [49].

3.2.1.1 Global Navigation Satellite System (GNSS)

The GNSS is a constellation of satellites which provides global coverage of signals from space transmitting positioning and timing data. Examples of GNSS are the USA's NAVSTAR GPS, Russia's Global'naya Navigatsionnaya Sputnikovaya Sistema (GLONASS), and the new Europe's Galileo system. The accuracy and integrity of GNSS can be greatly enhanced by the use of augmentation information derived from various sources such as: Space Based Augmentation Systems (SBAS) (for example the European Geostationary Navigation Overlay Service (EGNOS) in Europe and Asia, Wide Area Augmentation System (WAAS) in USA, Multi functional Satellite Augmentation System (MSAS) in Japan, as well as the GPS Aided Geo Augmented Navigation (GAGAN) system in India).

3.2.1.1 Description of GPS

GPS consist of three segments showed in Fig. 3.1: the space segment is formed by the satellite constellation, the control segment is formed by the monitoring stations and the user segment is formed by the GPS receivers.

The Space Segment

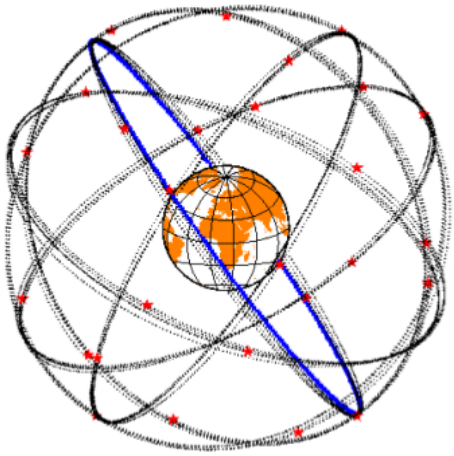

Figure 3.1: The orbital configuration of GPS Satellites (taken from http//www.google.com/images q = GPS+constellation channels).

The Space Segment consists currently of 32 GPS satellites (PRN:1 - 11, 13 - 18, 20, 21 and 23 -32) arranged in 6 orbital planes located at the altitude of 20,200 km inclined at 55° to the equator. The coverage provided by the GPS constellation which provide information for determining the position of the satellite, its distance from the user and satellite clock error, ensures a minimum of 4 satellites and maximum of 11 satellites visible at anytime, anywhere in the world. The orbital period of satellite is approximately 11hr 58min. Therefore a GPS satellite completes 2 revolutions in 23 hr 56 min as a result of this, the satellite appears over the same geographical location on the Earth's surface every day (i.e. minus 4 minutes).

The Control Segment

The Control Segmen tracks each satellite and periodically sends the corrections of ephemeris and clock which are analyzed continuously by monitoring stations around the globe, that are in Hawaii, Ascension Island, Kwajalein, and Diego Garcia Fig. 3.2. The monitoring stations are analyzed remotely by a Master Station at Colorado Springs which provides commands and control functions. The monitoring stations are equipped with communication facilities to 22 transmit data to the master station via terrestrial transmission (S band). Some functions of the Master station include the following:

1. monitor the satellite orbits;
2. monitor and maintain the health of the satellites;
3. keep the GPS time;
4. calculate the satellite ephemeris and clock parameters;
5. update the navigation messages from satellites, and
6. control maneuvers to maintain satellites in orbit and re-allocate satellites.

The User Segment

The user segment consists of receivers used by both military and civilians. The receiver is made up of hardware and processing software for positioning in three dimensions, navigation, and timing applications. This is possible by making use of the signals transmitted by the constellation of GPS. Today there are several hundred of GPS receivers stations

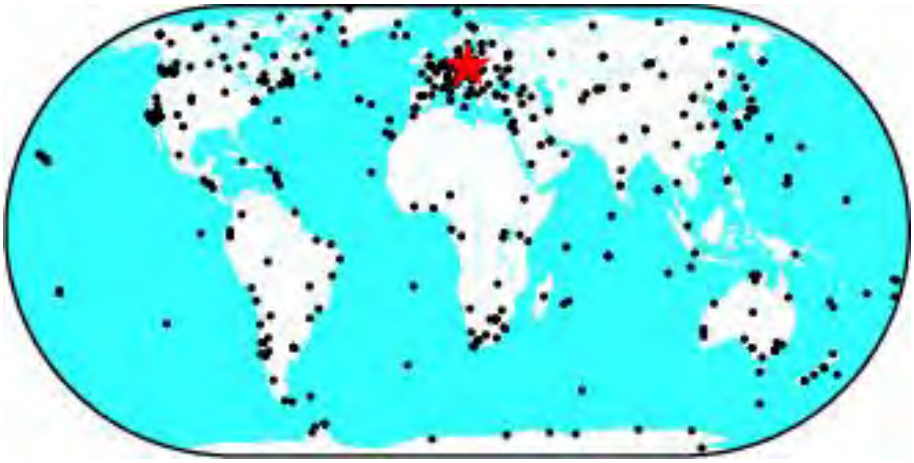

Figure 3.2: IGS network of permanent GPS tracking stations (Source: http://igscb.jpl.nasa.gov/network/site/wroc.html).

around the world. Fig. 3.2 represent the distribution of permanent global GPS sites maintain by the International GPS Service, which consists of more than 300 stations. It is clear evidence from the Fig. 3.2 that the density distribution of the receivers is more at the

northern hemisphere compared to the southern hemisphere. The data used for this study were collected from both IGS and can be obtained via ftp://garner.ucsd.edu/pub/rinex/.

3.2.2 Methods to obtain the TEC

There are several methods to obtain the TEC over the reference station. In this work TEC was obtained from dual frequency method and the IGS (International GPS Service) TEC map. This GPS station is a non-IGS station with in situ data obtained in Rinex file format. IGS TEC map are obtained from IGS data base where TEC map files are in IONEX (IONosphere Exchange) file format. It is important to underline that the used Rinex file contains data recorded at 30 seconds interval while IONEX file contains data recorded at an interval of two hours.

3.2.2.1 Dual frequency method

TEC is significant in determining scintillation and group delay of a radio wave through a medium. The basic GPS observables are code psedoranges and carrier phases. Ionospheric TEC is characterized by observing carrier phase delays of received radio signals transmitted from satellites located above the ionosphere, often using GPS satellites. GPS satellites transmit electromagnetic waves for positioning on two frequencies which is L_1 (1575.42 MHz) and L_2 (1227.60 MHz) allowing receivers equipped with dual frequency operation to be used. This enables us to extract the ionosphere TEC along the line of sight, from satellite to receiver. In this work, the TEC is observed at the F layer because this region has the highest variability of free electrons, causing the greatest effect on GPS received signal compared to other layers. More than two-third of electron concentration are located at F_2 layer. This method is conducted by going through several processes.

The process of extracting data from RINEX (Receiver Independent Exchange) file was done by using Matlab programming language where by the RINEX file was obtained from the GPS receiver. The program will analyse and extract the information needed in calculating the TEC from the observation and navigation RINEX file. The result will

show the graph of elevation angle, different phase, different delay, slant TEC (STEC) and vertical TEC (VTEC) versus time. This data of (VTEC) were used since its value is not depending on the location of satellite receiver compared to STEC.

Dual-frequency carrier phase and code-delay GPS observations are combined to obtain ionospheric observables related to the (STEC) along the satellite-receiver line of sight (LOS). The pseudorange is the measure of the distance between the satellite and the receivers antenna. The pseudorange is calculated by multiplying the apparent travel time of the GPS signal from a satellite to the receiver with the speed of light. This is not equal to the real satellite-receiver range because of a time difference between receiver and satellite clocks errors and transmitting media delay effects, hence the name pseudorange (false range) Pseudorange is applicable to P(Y)-codes and C/A-codes.

The pseudorange equation in units of length can be expressed as:

$$P_r = c(t_r - t^s) = c\tau_r^s = \rho_r^s + c(\delta t_r - \delta t^s) + I + T + mpp + \varepsilon \tag{3.2.1}$$

where P_r is pseudorange measured at receiver; c is speed of light in vacuum, t^s is transmission time of signal measured by time frame of satellite, s; t_r is reception time of signal measured by the clock of receivers r; τ_r^s is signal travelling time, ρ_r^s is LOS range from satellite antenna and receiver antenna, δt^s, δt_r is satellite and receiver clock error due to the difference in system time; I is ionospheric induced error; T is tropospheric induced error; mpp is multipath error and ε is noise or random error. Carrier phase is the measurement of the phase difference between the carrier signal generated by the receivers internal oscillator and the carrier signal transmitted from a satellite.

The basic equation for the carrier phase measurement is

$$L_r = \rho_r + c(\delta t_r - \delta t^s) - T + \lambda N_r^s + mpL + \varepsilon \tag{3.2.2}$$

where L_r is phase measurement in units of length, N_r^s is integer ambiguity between the satellite and receiver, mpL is multipath error. The true range or geometric range can be

represented by:

$$\rho_r^s = \sqrt{(X^s - x_r)^2 + (Y^s - y_r)^2 + (Z^s - z_r)^2} \tag{3.2.3}$$

where X, Y and Z are the satellite coordinates, x, y and z are the receiver coordinates. Dual band GPS receivers were considered in the measurable linear combination (LC). Dual frequency observations can be used to measure the ionosphere delay. This delay can then be removed from the measurements by combining the frequencies, L_1 and $L2$. Ionosphere delay can then be removed from the measurements by combining the frequencies and providing the Linear Combination (LC) solution. All observables have the dimension of length, terms due to noise and multipath are not explicitly shown, and higher-order ionospheric terms are ignored:

$$L_1 = \rho - I_1 + \lambda_1 N_1 \tag{3.2.4}$$

$$L_2 = \rho - (\frac{f_1^2}{f_2^2})I_1 + \lambda_2 N_2 \tag{3.2.5}$$

$$P_1 = \rho + I_1 \tag{3.2.6}$$

$$P_2 = \rho + (\frac{f_1^2}{f_2^2})I_1 \tag{3.2.7}$$

Where ρ is non dispersive delay, contains LOS, clocks and troposphere bias, I_1 is dispersive delay of first frequency and N_1, N_2 is integer ambiguities on L_1 and L_2. The integrated TEC from the receiver to the satellite is proportional to the accumulated effect by the time the signal arrives at the receiver. This affects the GPS range observables: a delay is added to the code measurements and advance to the phase measurements. To achieve very precise positions from GPS, this ionospheric delay or advance must be taken into account. GPS satellites continuously transmit signals centered on two carriers L_1 and L_2 with frequencies f_1 and f_2. A GPS operates on two different frequencies f_1 and f_2 , which are derived from the fundamental frequency of = 10.23 MHz:

$$f_1 = 154.fo = 1575.42MHzand \tag{3.2.8}$$

$$f_2 = 120.fo = 1227.60MHz \tag{3.2.9}$$

A dual-frequency GPS receiver can measure the difference in ionospheric delays between the L_1 and L_2 of the GPS frequencies, which are generally assumed to travel along the same path through the ionosphere. The error or effect of 1st order due to ionosphere in pseudorange along the satellite direction referred to as the ionospheric delay (I) can be calculated from the refractive index

$$\Delta r = \int_r^s (n-1)dI \tag{3.2.10}$$

where Δr is the group delay and n is the refractive index. The first-order refractive index (n) is given by: $\frac{1-40.3N}{f^2}$

$$TEC = \int_r^s NdI \tag{3.2.11}$$

where N is the electron density and 1 TEC unit $=10^{16}$ electrons/m^2 . Note that TEC is proportional to the ionospheric differential delay between $L1$ (1575.42Mhz) and $L2$ (1227.60MHz) signals. Thus, the group delay can be obtained as

$$P_1 - P_2 = 40.3TEC(\frac{1}{f_2^2} - \frac{1}{f_1^2}) \tag{3.2.12}$$

Where P_1 and P_2 are the group path lengths corresponding to the high GPS frequency ($f_1 = 1575.42MHz$) and the low GPS frequency ($f_2 = 1227.6MHz$), respectively. The TEC can also be obtained by writing Eq. (3.2.10) as:

$$TEC = \frac{1}{40.3}(\frac{f_1^2 f_2^2}{f_1^2 - f_2^2})(P_2 - P_1) \tag{3.2.13}$$

if dual frequency receiver measurements are available; where (P_1 and P_2) are the pseudoranges measured in $L_1 and L_2$, respectively. TEC can be divided into two parts. There are: Slant TEC (STEC); Vertical TEC (VTEC). Slant TEC is a measure of the total electron content of the ionosphere along the ray path from the satellite to the receiver, represented in Fig. 3.4. Although STEC is measured at differing elevation angles, usually the VTEC is

modelled. VTEC enables TEC to be mapped across the surface of the Earth.
TEC measurements are taken from different GPS satellite observed at arbitrary elevation angles. This causes the GPS signals to cross largely different portion of the ionosphere. To compare the electron contents for paths with different elevation angles, the STEC must be transformed into equivalent vertical content or VTEC by dividing it by the secant of the elevation angle at a mean ionospheric height, which usually taken to be between 350 and 450 km. Generally by referring to Fig. 3.3, the slant TEC, STEC through a given sub- ionospheric point is obtained from Eq. (3.2.12).

3.2.2.2 Mapping Function

Precision monitoring of ionosphere will have profound implications in almost all areas of GPS user communities. The ionospheric mapping function is one of the first assumptions to consider typically when ionospheric corrections are estimated or applied from Global Navigation Satellite System (GNSS) data. The typical assumption in many GNSS imaging and navigation systems is to consider a fixed mapping function constant, and associated to a 2D distribution of electron content at a given effective height (typically some value between 300 and 500 km). The line-of-sight TEC values were converted to VTEC values using a simple mapping function and were associated to an ionospheric pierce point (IPP) latitude and longitude, assuming the ionosphere to be compressed into a thin shell at the peak ionospheric height of 350 km as illustrated in Fig. 3.3. The thin shell model was used and its height is the effective height which is taken as the ionospheric pierce point altitude. Generally, the ionosphere can be divided into several layers in altitude according to electron density, which reaches its peak value at about 350 km in altitude. The thin layer model currently used in GPS has deficiencies resulting from conversion of slant TEC to effective vertical TEC. The deficiencies come from in appropriate attribution of the thin shell height. This conversion introduces a few errors in the middle latitude where electron density is small. But it many result in obvious error at low latitude with large electron

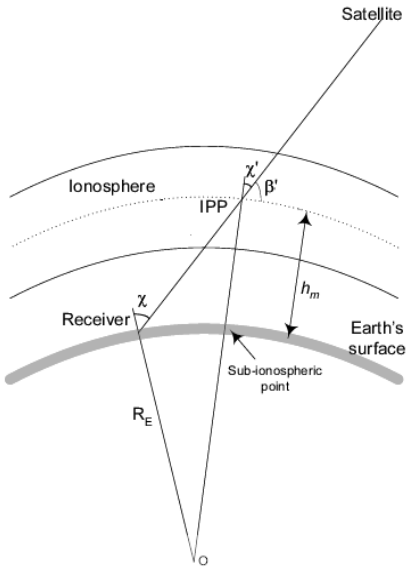

Figure 3.3: Ionospheric Single Model (SLM) (Source: Schaer 1996)

density and great gradient [50]. Usually, the ionospheric delay resulting from observation noises, less than $1TECU$, is omitted. It is assumed that, in the two- dimensional spherical shell model, the majority of electron density is concentrated in a thin layer with a height of 350-450 km above the surface of the Earth. Generally by referring to Fig. 3.3, STEC through a given sub-ionospheric point is obtained from Eq. 4.3.12

$$TEC_v = TEC_s(\cos\chi\prime) \tag{3.2.14}$$

where TEC_s is the value of slant TEC, $\chi\prime$ is the difference between 90 and zenith angle (90°-χ). In some literature this is called the elevation-dependent single layer (or thin shell) model mapping function, SLM where can be written as

$$F(X) = \frac{TEC(X)}{TEC(0)} = \frac{1}{cos\chi\prime(or sin\beta\prime)} = \frac{1}{\sqrt{1 - sin^2\chi\prime}} \tag{3.2.15}$$

$$sin\chi\prime = \frac{R_e}{R_e + h_m} sin\chi \tag{3.2.16}$$

where R_e is the mean earth radius, h_m is the height of maximum electron density, and χ and $\chi\prime$ are the zenith angles at the receiver site and at the IPP (or $\beta\prime$ is the elevation

angle at IPP), respectively. χ can be calculated from a known satellite position and the approximate coordinates of the receiver location. For h_m , in general the value is taken as the height corresponding to the maximum electron density at the F_2 peak. The peak altitude ranges from 250 to 350 km at mid-latitudes and from 350 to 500 km at equatorial latitudes. Typical value for R_e and h_m are set to 6371 and 450 km, respectively. The more precise mapping function according to Schaer et al., [40] and currently applied in the IGS Global TEC map is the modified single layer model, M-SLM. This is defined as:

$$sin\chi\prime = \frac{R_e}{R_e + h_m} sin(\alpha\chi) \tag{3.2.17}$$

where α is correction factor which is close to unity. The value is chosen to be 0.9782 when using R_e and h_m as 6371 and 506.7 km, respectively and assuming a maximum zenith angle of 80°. $F(\chi)$ is also known as the slant or obliquity factor in the Klobuchar model and varies from 1 to slightly above 3 at $h_m = 350$ km. For low elevation angles slant TEC can reach until 3 times the value of TEC at zenith. However the oblique-to-zenithal thin shell conversion including the determination of h_m is still being developed further. It has also been suggested that h_m should be taken to be between 600 and 1200 km which is greater than the commonly adopted value. If this is correct, assuming a lower value could produce an error of 15 to 30% or more in TEC.

3.2.2.3 Carrier phase levelling process

GPS signals can be used to extract ionospheric parameters such as TEC. For single frequency GPS users, models of the ionosphere such as the Klobuchar model [51], which is also known as the GPS broadcast model, have been constructed utilizing ionospheric parameters given in the GPS broadcast message. It is represented by a third degree polynomial where the coefficients of the polynomial are transmitted as part of the broadcast message header. The TEC can also be obtained as in Eq. 3.2.7, if dual frequency receiver measurements are available. As the TEC between the satellite and the user depends

on the satellite elevation angle, this measurement is called STEC. The TEC varies with times and over the space, and it depends on the solar activity, user location and the PRN elevation angle.

In practice, calculation of TEC by the above means, using pseudorange data only, can produce a noisy result. It is desirable to also use the relative phase delay between the two carrier frequencies in order to obtain a more precise result. Differential carrier phase gives a precise measure of relative TEC variations but because the actual number of cycles of phase is not known, absolute TEC cannot be found unless pseudorange is also used. Pseudorange gives the absolute scale for TEC while differential phase increases measurement precision. The TEC data derived from GPS pseudorange measurements have a large uncertainty because the pseudorange has high noise level. In contrast, the noise level of carrier phase measurements is significantly lower than the pseudorange ones. To reduce the effect of pseudorange noise on TEC data, GPS pseudorange data can be smoothed by carrier phase measurements. For example is by using carrier phase smoothing technique, which is also often referred to as carrier phase levelling. Carrier phase levelling or phase smoothing is essentially some combination of the noisy code pseudorange with the comparatively smooth varying carrier phase. The carrier phase contains much smaller measurement error than pseudoranges, so that ionospheric TECs can be obtained by carrier phase smoothing the pseudoranges [52]. This was done as shown below: Firstly, the phase observations, measured in cycles, are scaled to units of length by multiplying with the wavelength. Because the phase measurements are ambiguous, so the phase derived slant delay, obtained from geometry free linear combination, L_4 calculated from Eq. (3.2.16) was scaled to zero relative range error at the first epoch. This eliminates the integer ambiguity provided there are no cycle slips.

$$L_4 = L_1 - L_2 = (\frac{1 - f_1^2}{f_2^2})I_1 + (\lambda_1 N_1 - \lambda_2 N_2) \tag{3.2.18}$$

To eliminate the code multipath effect that is normally seen at both ends of the path or at low elevation angles, the code differential delay was fitted at the higher elevation angles.

GPS Total Electron Content (TEC) Prediction at Ionosphere Layer over the Equatorial Region This was done by defining a shift value and was added to the relative phase to fit the code differential delay. This results in the absolute differential delay and the remaining noise was discarded. The smoothed differential delay (with less noise and multipath) was then translated to the absolute STEC by multiplying with a constant (see Eq. 3.2.11). A mapping function, SLM isused together with Eq. (3.2.12) to convert TEC to the vertical from the slant value. For a good description on the determination of absolute TEC from dual frequency GPS measurements refer to [53].

3.2.3 IGS (International GPS Service) TEC map

Bernese GPS Software (BGS) was used to map the ionosphere in this work. BGS is commonly used by scientists for research and education, survey agencies responsible for high-accuracy GNSS surveys, agencies responsible for maintaining arrays of permanent GPS receiver and also commercial users with complex applications demanding high accuracy, reliability and high productivity [54]. TEC map has gained much attention in the recent years because of the ionospheric effects to the GPS-based navigation application. A range delay caused by the ionosphere during quiet and disturbed geomagnetic days can be approximated by using the measurements of TEC map. TEC ionopheric values and maps can be delivered by the International GPS Service (IGS). IGS has developed the global ionospheric gridded data representing the TEC over the whole globe. Analysis centres deliver their results of VTEC and DCBs in the IONosphere Exchange (IONEX) format [55]. In this new version of BGS, PPP (precise point positioning) was processed using BPE. BPE (Bernese Processing Engine) consists of data, user scripts and four process control file (PCF) where one of the PCF is PPP. PCF in PPP mode has been selected to run PPP. In this PPP.PCF, regional ionosphere model is generated and stored in Bernese ionosphere file and in IONEX file using GPS Estimation (GPSEST) program. GPSEST

is the program that able to generate TEC maps in IONEX [55]. GPSEST program is used to model and estimate the ionosphere. In GPSEST program, geometry-free linear combination from the zero-difference code observations was used because it principally contains ionospheric information. Geometry-free linear combination of this un-differenced GPS observations is then applied in GPSEST to generate TEC map.

A MSLM (Mapping single layer model) was used for mapping the TEC, approximated by a spherical layer with infinitesimal thickness assuming that all free electrons are concentrated in altitude, H, above the spherical Earth. The altitude H of this idealized layer is set to 350 km. Based on this model, TEC values were calculated in geographic reference system which was able to produce the epoch-specific instantaneous regional maps of the ionosphere. Using MSLM noted above, a vertical TEC can be obtained at IPP. It can be shown that a single GPS receiver can probe the ionosphere in a radius of 960 km assuming 10°elevation cut-off angle and 450 km height. This proved that PPP technique can be used to determine TEC. With the new BGS version 5.0; PPP technique is now available to produce ionosphere maps. PPP is known as a valuable tool to provide an accurate position anywhere on Earth, also for investigating many geophysical processes at the millimetre level.

3.2.3.1 Application of IONEX TEC Maps

We may use three different procedures to compute the TEC E as function of geocentric latitude β, longitude λ and universal time t, when we have TEC maps

$$E_i = E(T_i) \tag{3.2.19}$$

where i=1,2,$\cdots$, n at our disposal:

simple take the nearest TEC maps $E_i = E(T_i)$ at epoch T_i:

$$E(\beta, \lambda, t) = E(\beta, \lambda) \tag{3.2.20}$$

where $|t - T_i| = \min$.

Interpolation between two consecutive TEC maps $E_i = E(T_i)$ and $E_{i+1} = E(T_{i+1})$

$$E(\beta, \lambda, t) = (\frac{T_{i+1} - t}{T_{i+1} - T_i})(E_i(\beta, \lambda)) + (\frac{t - T_i}{T_{i+1} - T_i})(E_{i+1}(\beta, \lambda)) \tag{3.2.21}$$

where $T_2 <= t < T_3$.

Interpolation between consecutive rotated TEC maps.

$$E(\beta, \lambda, t) = (\frac{T_{i+1} - t}{T_{i+1} - T_i})(E_i(\beta, \lambda\prime_i)) + (\frac{t - T_i}{T_{i+1} - T_i})(E_{i+1}(\beta, \lambda\prime_{i+1})) \tag{3.2.22}$$

where $T_i <= t < T_{i+1}$ and $\lambda\prime_i = \lambda + t - T_i$. The TEC maps are rotated by $t - T_i$ around Z-axis in order to compensate to a great extent correllation between ionosphere and the sun's position. Note method (1) can be refined accordingly by taking the nearest rotated maps: $E(\beta, \lambda) = E_i(\beta, \lambda\prime)$. From method (1) to method (2), one may expect an improvment of interpolation results, therefore we recommended to use the last approach(3).

Chapter 4

Result and Discussion

In this chapter we present the analysis of the results obtained using the IGS (International GPS service) data and the estimation techniques as presented in the previous chapters. The results are presented in this sections. In this section we discussed ionospheric TEC variation such as: the diurnal, seasonal, latitudinal and longitudinal TEC variation and Equatorial Ionization Anomaly (EIA). TEC variation.

4.1 Diurnal variation in TEC

To observe monthly diurnal, solar activity, longitudinal, latitudinal, seasonal TEC variation and the behavior of EIA, we have plotted contour plots of TEC for each month for a period of one years from 01 January to 31 December 2008. From the mapping we converted universal time to local time by using the equation:

$$T_z = \frac{LONG}{15}, LT = UT + T_z \tag{4.1.1}$$

where T_Z = time zone, LT = local time, LONG = longitude, UT = universal time. The diurnal variation in TEC is due to the regular rotation of the Earth about its own axis following the apparent movement of the Sun. However, the net diurnal change in the quiet day low latitude ionosphere mostly depend on the photoionization production and recombination losses associated with the local solar radiation and the field aligned diffusion of the transported electrons from the equator. Fig. 4.1 shows the typical

(a)

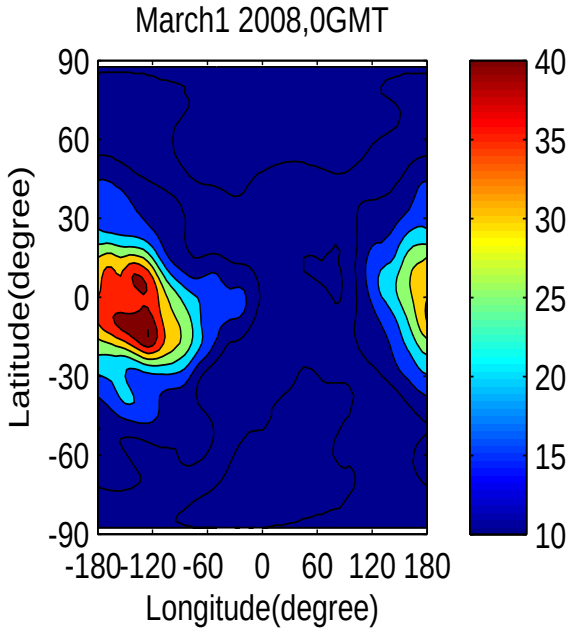
March1 2008,0GMT
Latitude(degree)
90
60
30
0
-30
-60
-90
-180 -120 -60 0 60 120 180
Longitude(degree)
40
35
30
25
20
15
10

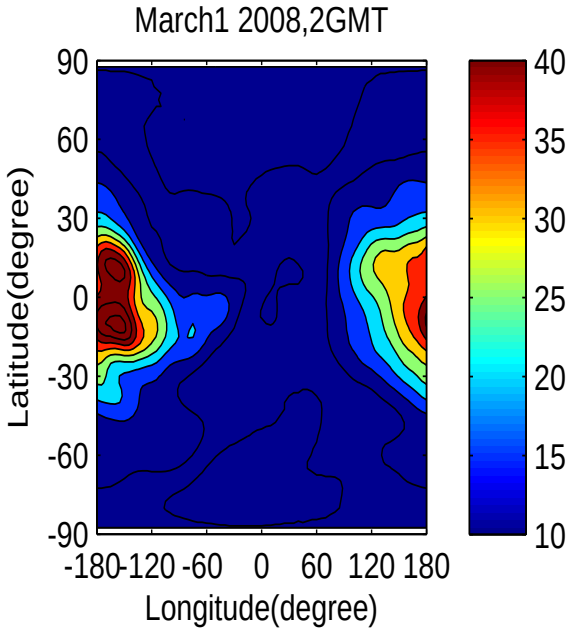
March1 2008,2GMT
Latitude(degree)
90
60
30
0
-30
-60
-90
-180 -120 -60 0 60 120 180
Longitude(degree)
40
35
30
25
20
15
10

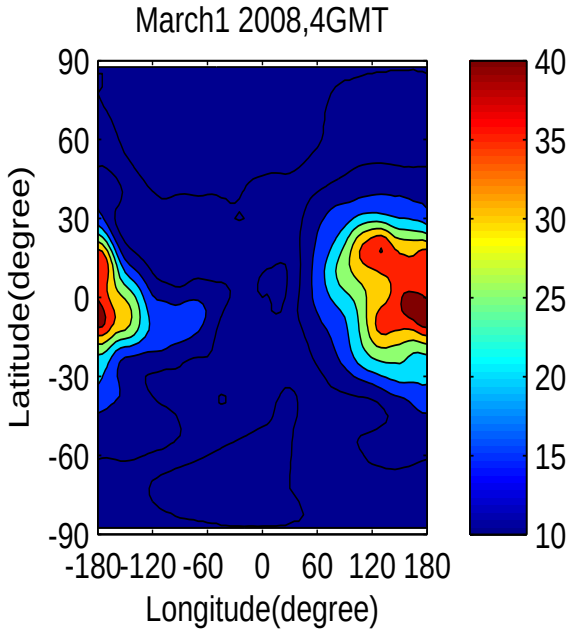
March1 2008,4GMT
Latitude(degree)
90
60
30
0
-30
-60
-90
-180 -120 -60 0 60 120 180
Longitude(degree)
40
35
30
25
20
15
10

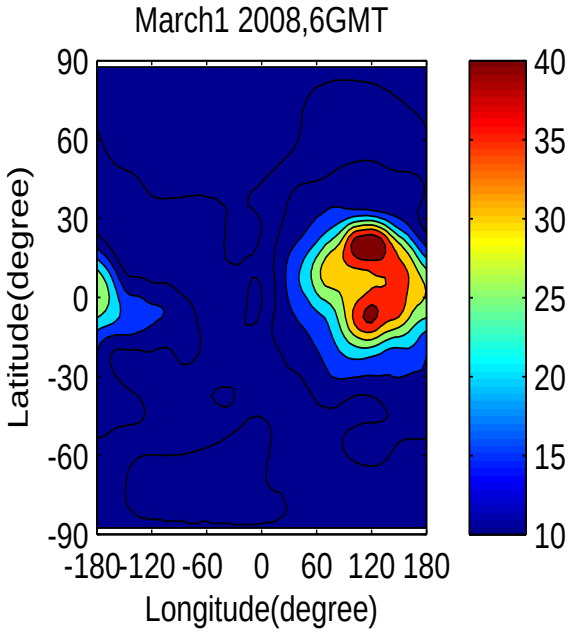
March1 2008,6GMT
Latitude(degree)
90
60
30
0
-30
-60
-90
-180 -120 -60 0 60 120 180
Longitude(degree)
40
35
30
25
20
15
10

(b)

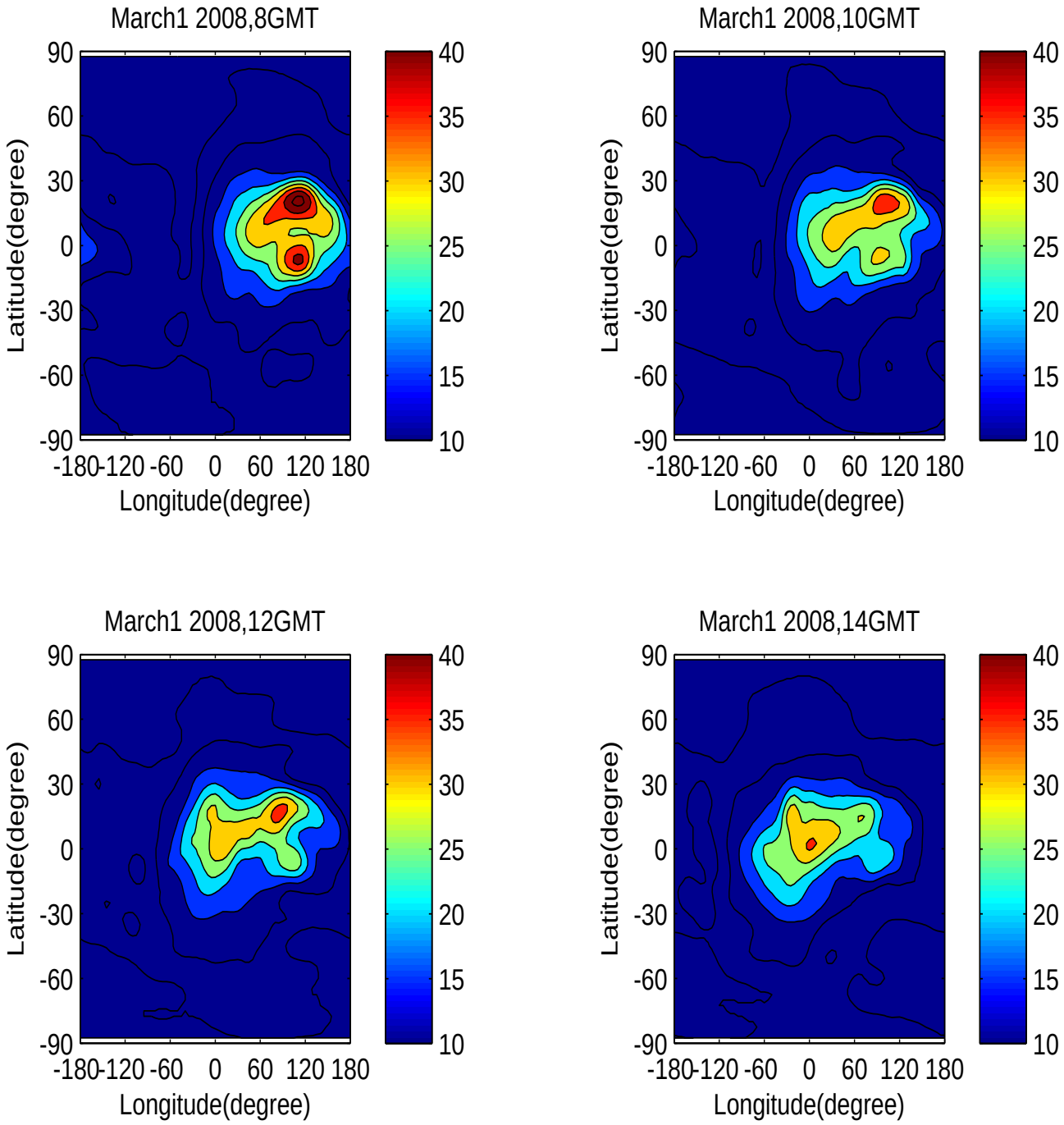
March1 2008,8GMT
March1 2008,10GMT
March1 2008,12GMT
March1 2008,14GMT
Latitude(degree)
Longitude(degree)
90
60
30
0
-30
-60
-90
-180 -120 -60 0 60 120 180
40
35
30
25
20
15
10

(c)

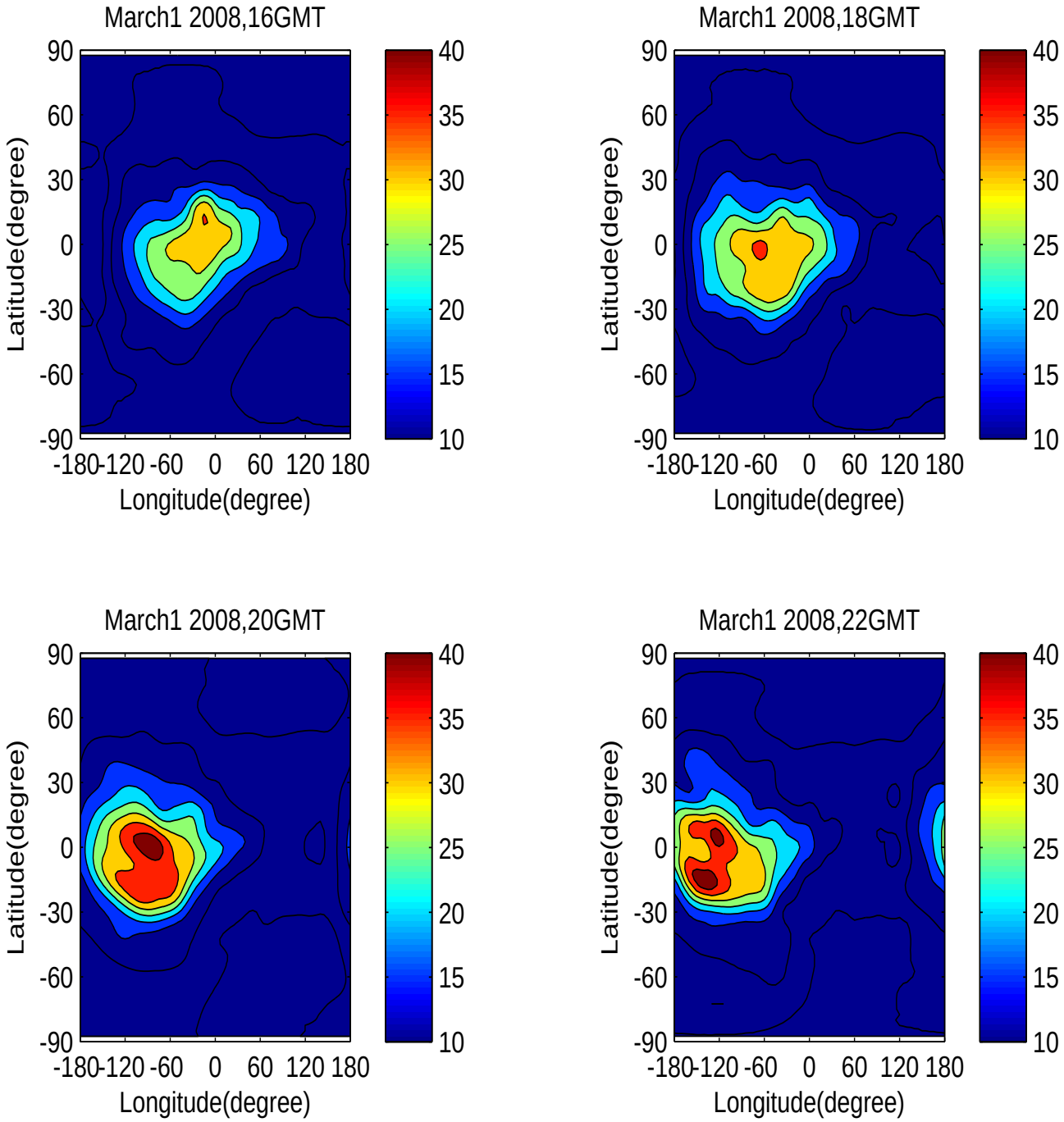

Figure 4.1: Latitude - longitude cross-section of VTEC on March 1, 2008 every 2 hour.

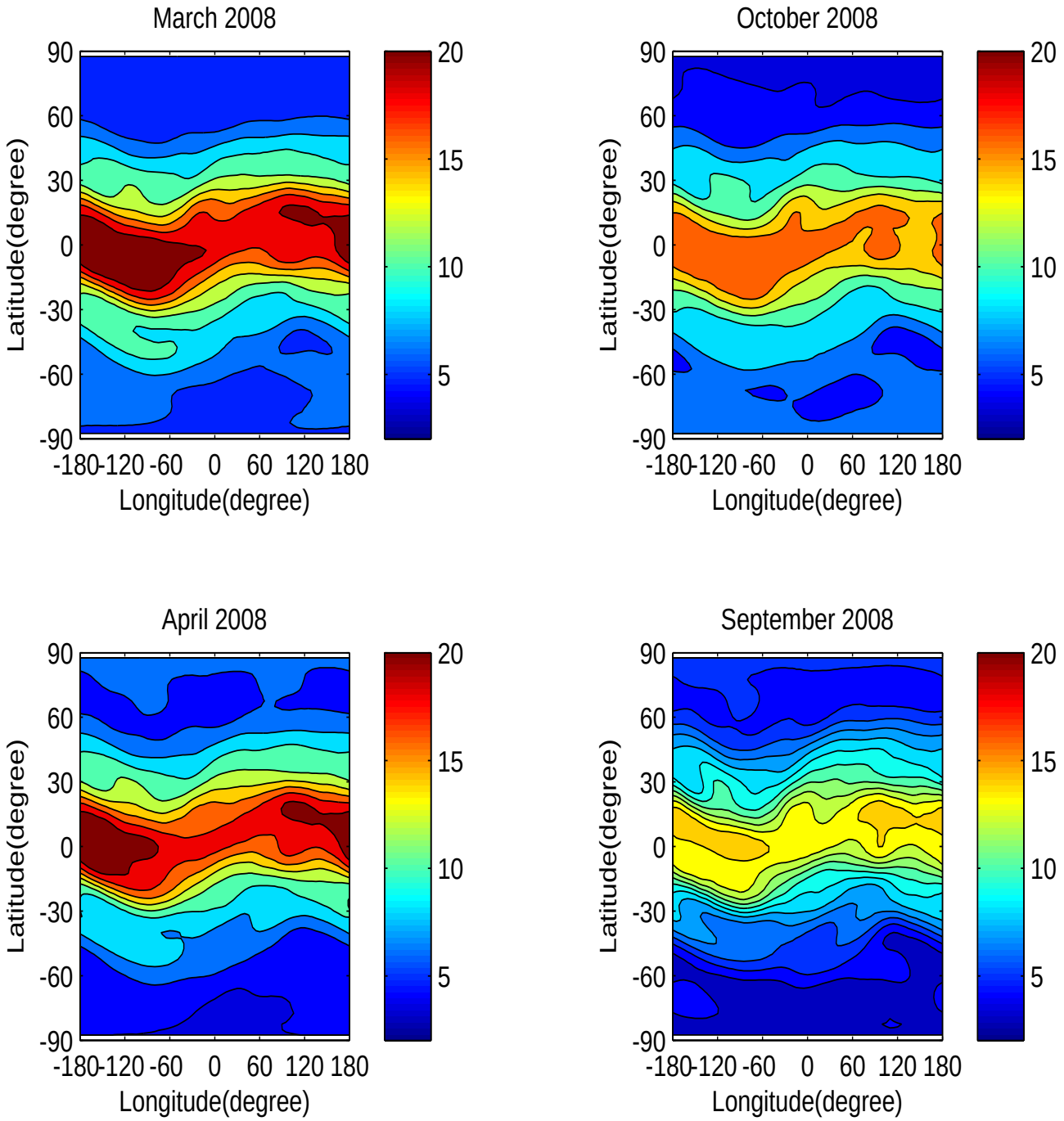

Figure 4.2: Latitude - longitude cross-section of VTEC for the Equinox months.

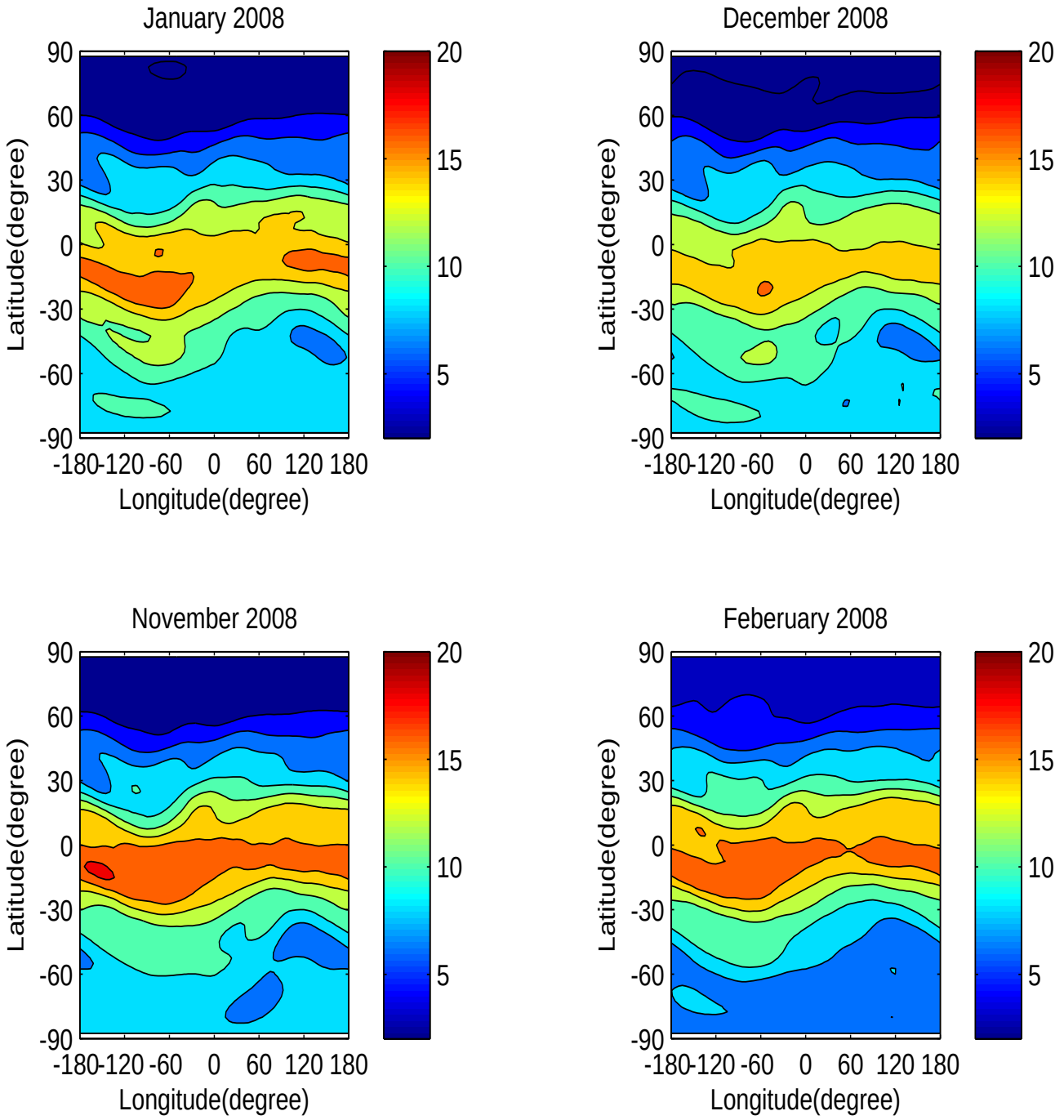

Figure 4.3: Latitude - longitude cross-section of VTEC for the Winter solstice months.

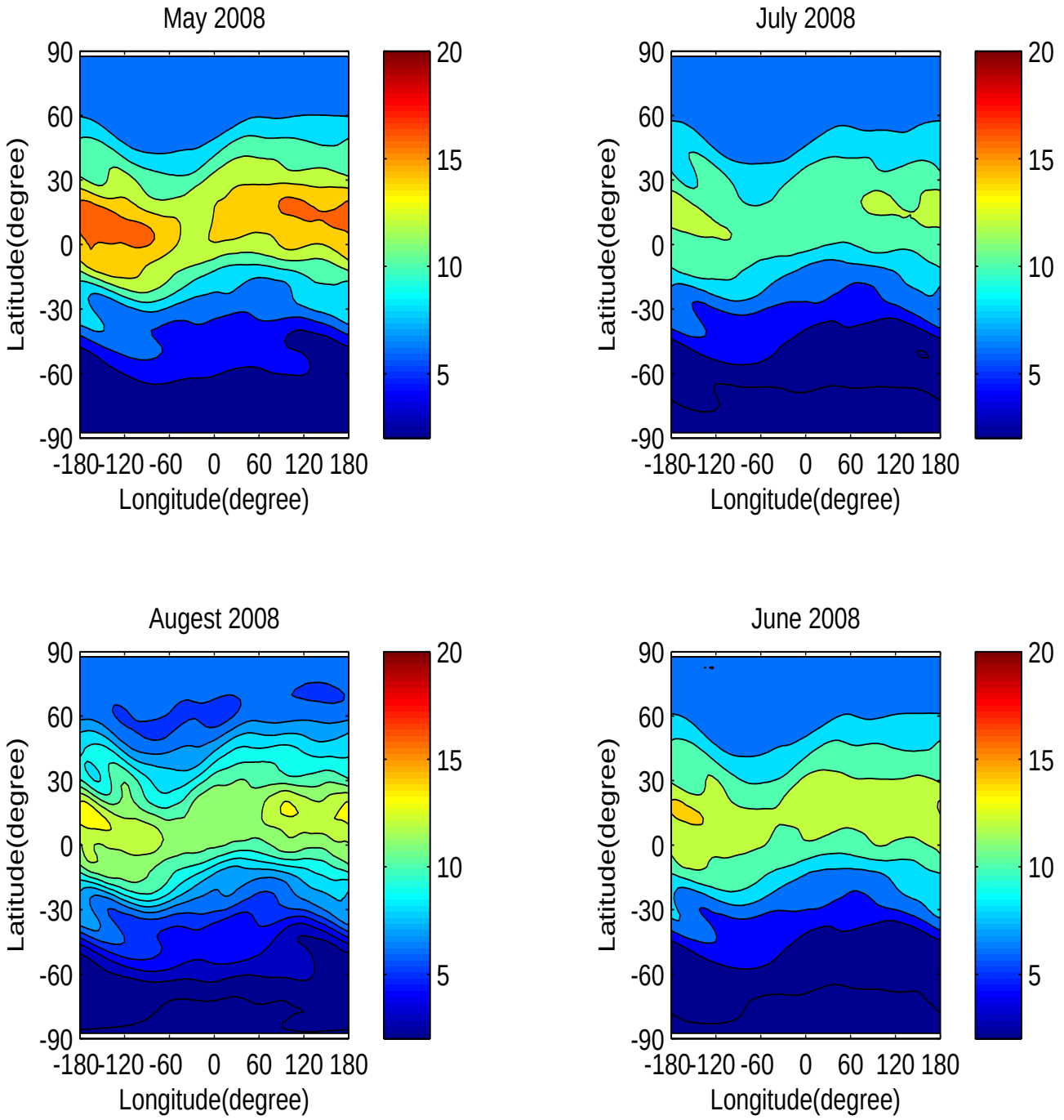

Figure 4.4: Latitude - longitude cross-section of VTEC for the Summer solstice months.

diurnal variation of TEC. TEC variation show typical diurnal characteristics such as TEC minimum at predawn and continuing increase with local sunrise attaining a maximum at local noon time followed by a decrease to a minimum during nighttime. As the sun rises, the ionization also increases which causes more concentration of electron near the F_2 peak at the ionosphere. Since TEC is directly related with the variation of monthly diurnal mean of TEC for the above mentioned 12 months has been shown in the contour plot of Figs. 4.2 - 4.4. The diurnal features mentioned above are reflected very well in this figure. From Figs. 4.1 - 4.4, the diurnal characteristics of TEC have seasonal, solar activity, geomagnetic and latitudinal dependence. The large variability imposed on the low latitude ionosphere during sunrise and sunset transition period is well understood. As the total magnetic field tube is very small at equatorial and low latitudes, the electron contents in the field tubes collapse rapidly after sunset in response to the low temperature in the thermosphere in the nighttime. Following the sunrise, the magnetic field tubes again get filled up rapidly because of their low volume resulting steep increase in ionization. As an example, data for twelve months of 2008 is shown in Figs. 4.2 - 4.4. Almost similar diurnal pattern is observed for all the months of different seasons. In general, the diurnal variation of TEC shows a short lived predawn minimum, a steady early morning increase, followed by an afternoon maximum and gradual fall after sunset. The observations of diurnal variation in TEC show that the time at which TEC reaches the diurnal peak vary from day to day and month to month. In general, the diurnal peak in TEC is found during 12:00-14:00 GMT hrs. Large variations in TEC are observed in daytime, while nighttime variations are found to be almost constant. Fig. 4.1 also shows Contour plots of longitude versus latitude in GMT time on 1 march 2008. It can be seen from the Fig. 4.1 that day minimum in TEC is obtained around 06:00 GMT hrs while day maximum occurs around 14:00 GMT hrs. The diurnal variation in TEC inside the EIA region as a minimum in the pre-sunrise hours, which sharply increases to maximum values between 12:00 to 16:00 GMT, while the peak at the equator occurs around 14:00 GMT. Beyond

the anomaly crest, the diurnal maximum value decreases with increasing distance from the geomagnetic equator. The nighttime TEC is almost flat attaining lowest value during 22:00 to 06:00 GMT, similar to that of mid-latitude region. As a result of $E \times B$ drift in the equatorial region, the electrodynamical lifting of equatorial plasma to F region heights, the maximum electron density exists in the $\pm 1520^{\circ}$ magnetic latitude and this region is known as crest region of EIA [Appleton 1946]. The equatorial ionization anomaly is a result of so called fountain effect which gives rise to lifting of the equatorial plasma to higher altitudes, during most of the daytime hours. This plasma subsequently diffuses along the geomagnetic field lines to either side of the magnetic equator, owing to the effects of ambipolar diffusion, gravity and pressure gradients, giving rise to an accumulation of ionization at the F-region altitudes around $\pm 15^{\circ}$ geomagnetic latitudes, resulting in the formation of crests of ionization, while simultaneously depleting the ionization over the magnetic equator . The low latitude exhibits lower value of TEC during May, June, July and August compared to the same months of the equatorial stations. This implies that the formation of EIA is weaker during these months which represents summer solstices. The EIA strength and characteristics can be observed. In almost all the months,TEC enhancement is larger. Longitudinal variation was observed shows slightly larger TEC enhancement in almost all the months. This is expected because closer to the equator and there is always a trough at the equator due to fountain effect as explained above. Anderson et al. [56] affirmed that the primary source of the enhancement at equatorial anomaly latitudes after sunset is the evening increase of the equatorial fountain. The strength of the EIA at sunset that is intensified by the prereversal electric field enhancement (PRE) is dependent on the solar activity.

(a)

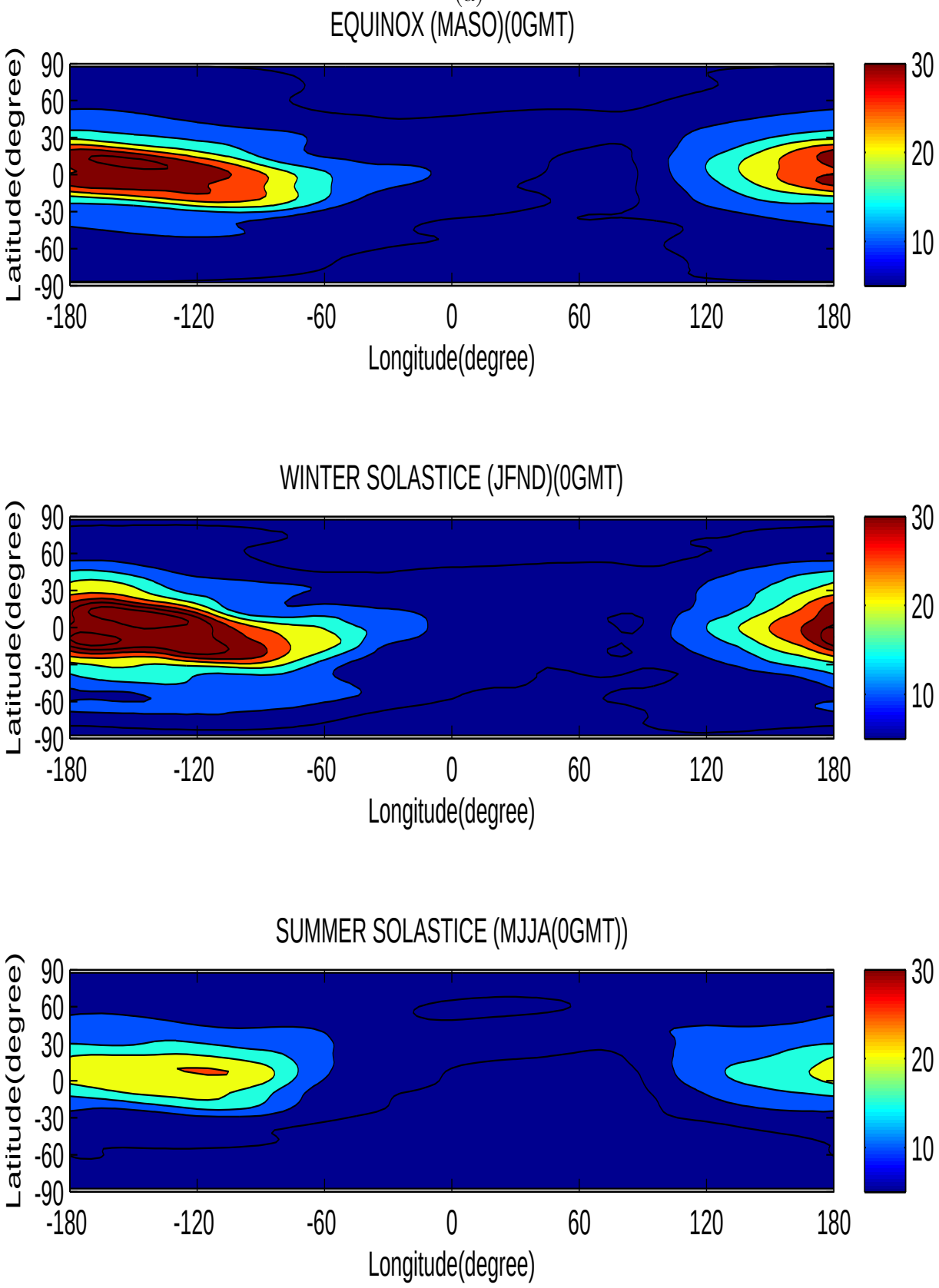
EQUINOX (MASO)(0GMT)
Latitude(degree)
90
60
30
0
-30
-60
-90
-180
-120
-60
0
60
120
180
Longitude(degree)
30
20
10
WINTER SOLASTICE (JFND)(0GMT)
Latitude(degree)
90
60
30
0
-30
-60
-90
-180
-120
-60
0
60
120
180
Longitude(degree)
30
20
10
SUMMER SOLASTICE (MJJA(0GMT))
Latitude(degree)
90
60
30
0
-30
-60
-90
-180
-120
-60
0
60
120
180
Longitude(degree)
30
20
10

(b)

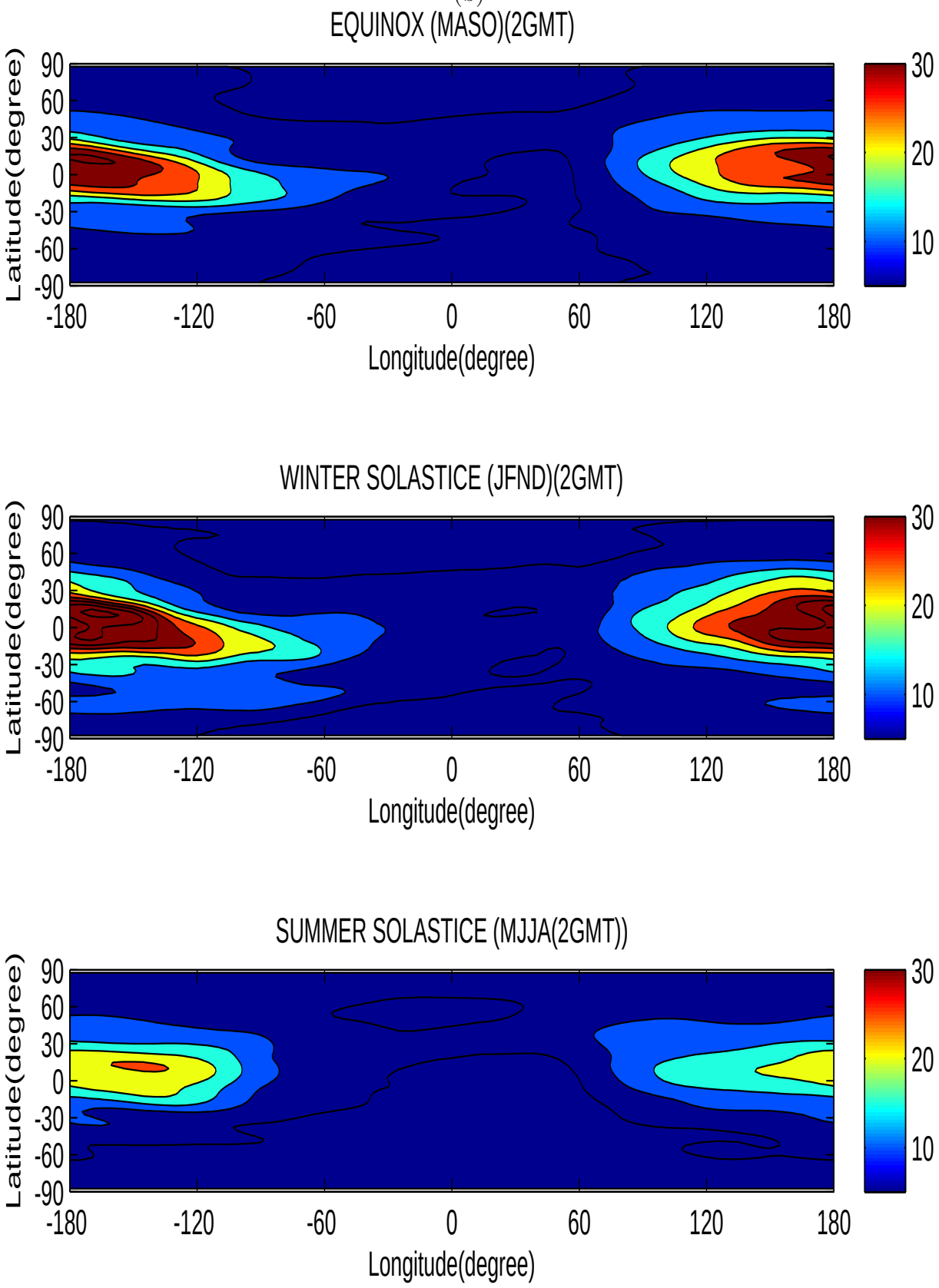
EQUINOX (MASO)(2GMT)
Latitude(degree)
90
60
30
0
-30
-60
-90
-180
-120
-60
0
60
120
180
Longitude(degree)
30
20
10
WINTER SOLASTICE (JFND)(2GMT)
Latitude(degree)
Longitude(degree)
SUMMER SOLASTICE (MJJA(2GMT))
Latitude(degree)
Longitude(degree)

(c)

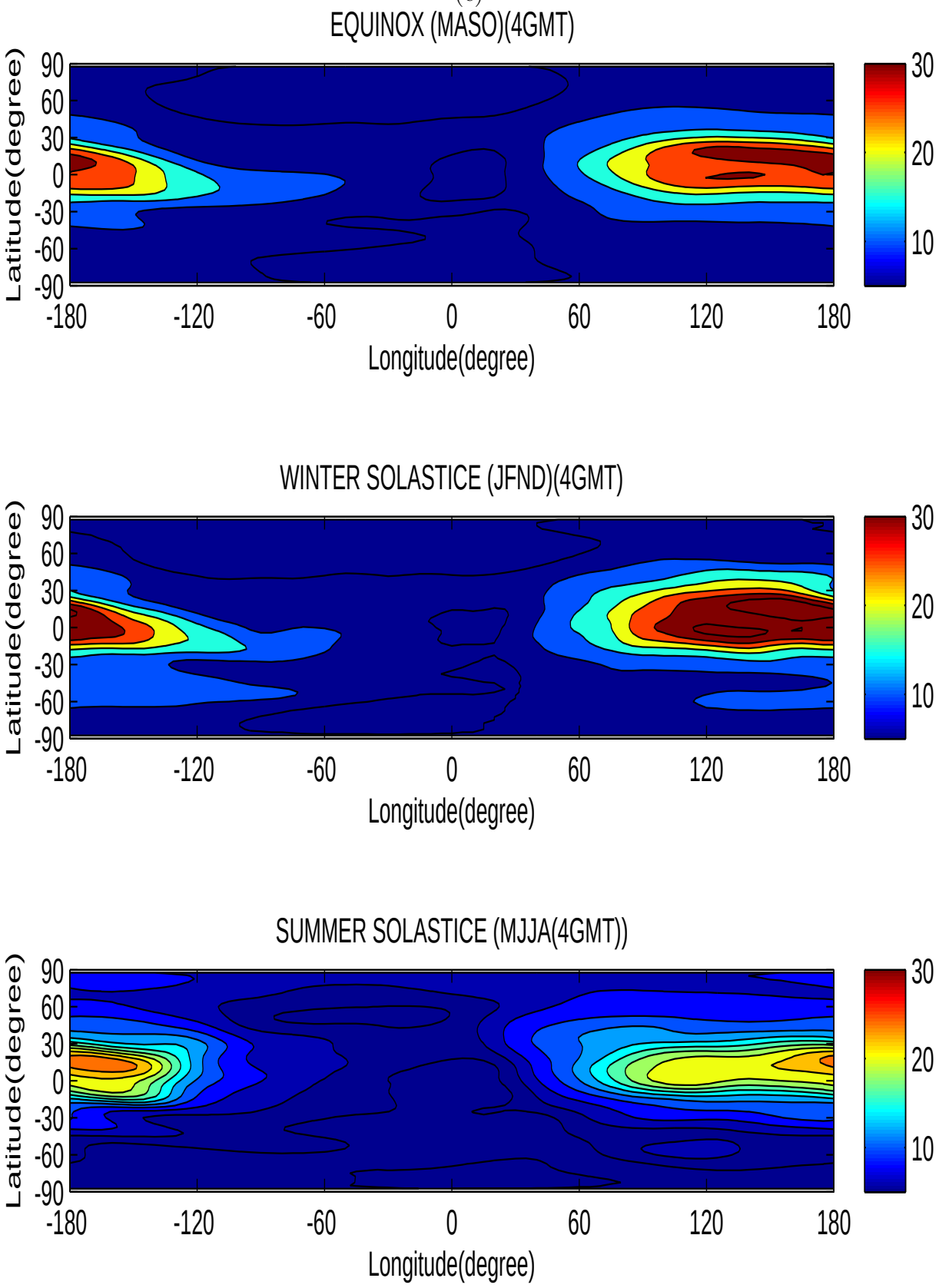
EQUINOX (MASO)(4GMT)
Latitude(degree)
90
60
30
0
-30
-60
-90
-180
-120
-60
0
60
120
180
Longitude(degree)
30
20
10
WINTER SOLASTICE (JFND)(4GMT)
Latitude(degree)
90
60
30
0
-30
-60
-90
-180
-120
-60
0
60
120
180
Longitude(degree)
30
20
10
SUMMER SOLASTICE (MJJA(4GMT))
Latitude(degree)
90
60
30
0
-30
-60
-90
-180
-120
-60
0
60
120
180
Longitude(degree)
30
20
10

(d)

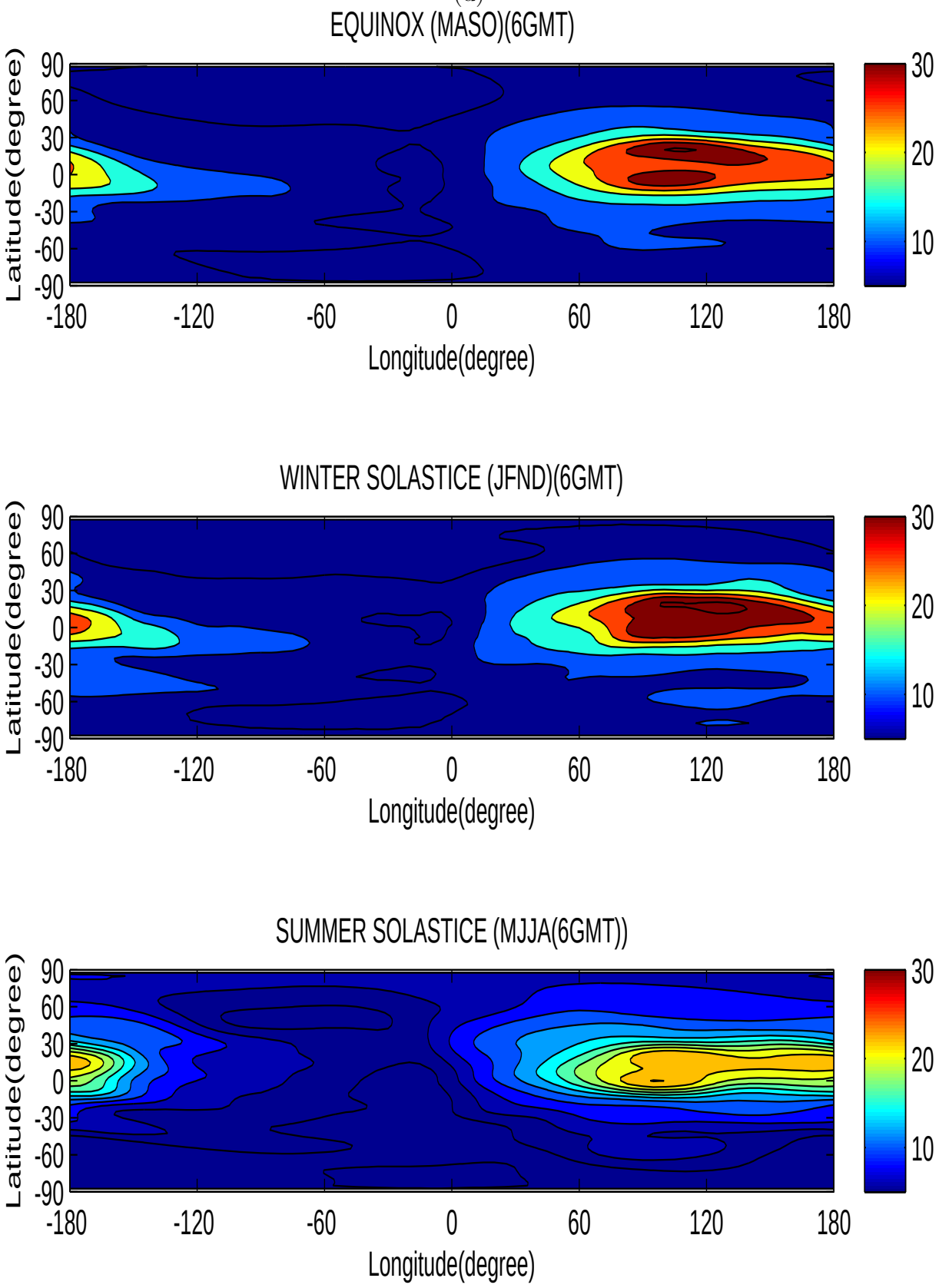
EQUINOX (MASO)(6GMT)
Latitude(degree)
90
60
30
0
-30
-60
-90
-180
-120
-60
0
60
120
180
Longitude(degree)
30
20
10
WINTER SOLASTICE (JFND)(6GMT)
Latitude(degree)
90
60
30
0
-30
-60
-90
-180
-120
-60
0
60
120
180
Longitude(degree)
30
20
10
SUMMER SOLASTICE (MJJA(6GMT))
Latitude(degree)
90
60
30
0
-30
-60
-90
-180
-120
-60
0
60
120
180
Longitude(degree)
30
20
10

(e)

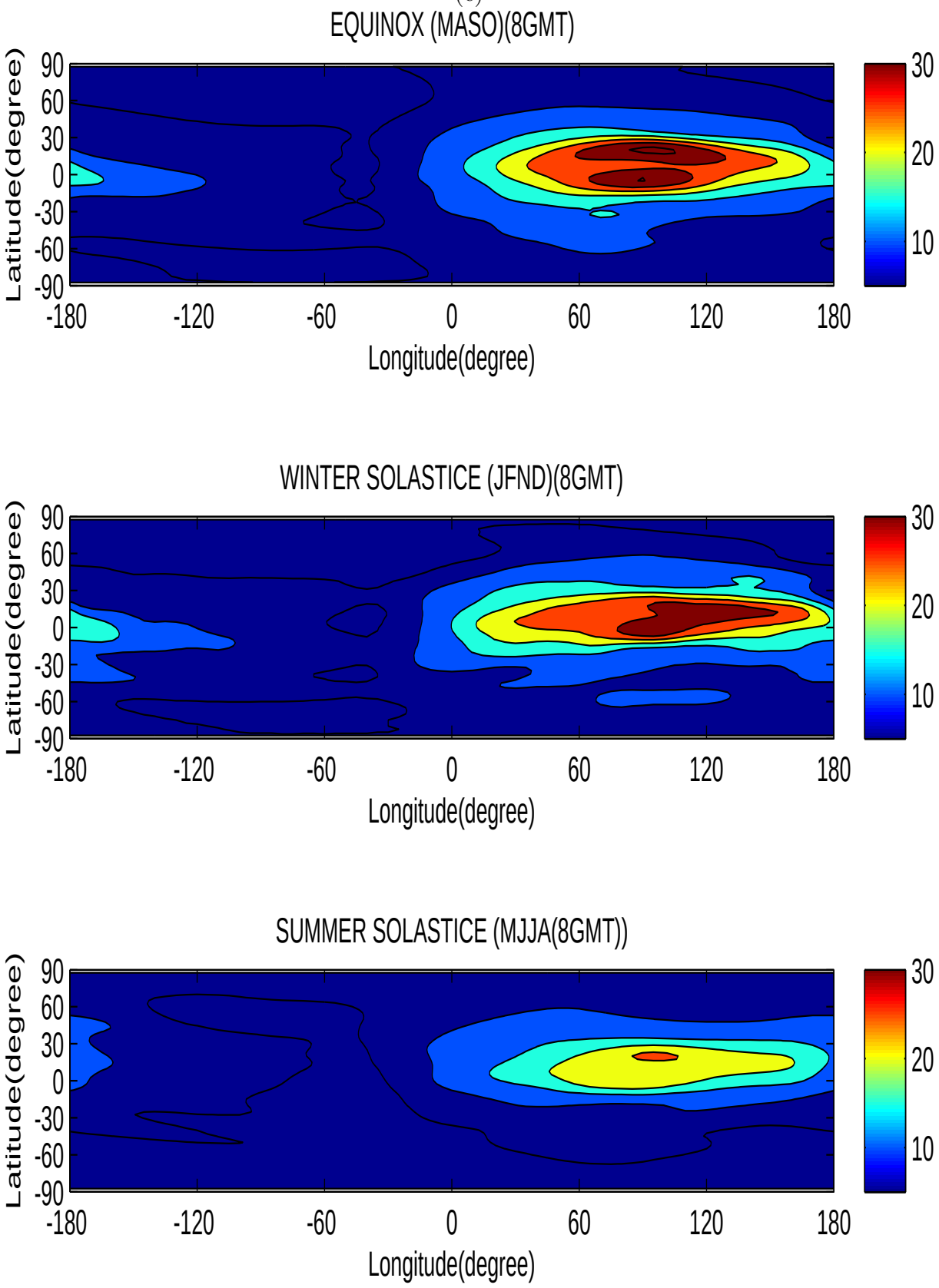
EQUINOX (MASO)(8GMT)
Latitude(degree)
90
60
30
0
-30
-60
-90
-180
-120
-60
0
60
120
180
Longitude(degree)
30
20
10
WINTER SOLASTICE (JFND)(8GMT)
Latitude(degree)
Longitude(degree)
SUMMER SOLASTICE (MJJA(8GMT))
Latitude(degree)
Longitude(degree)

(f)

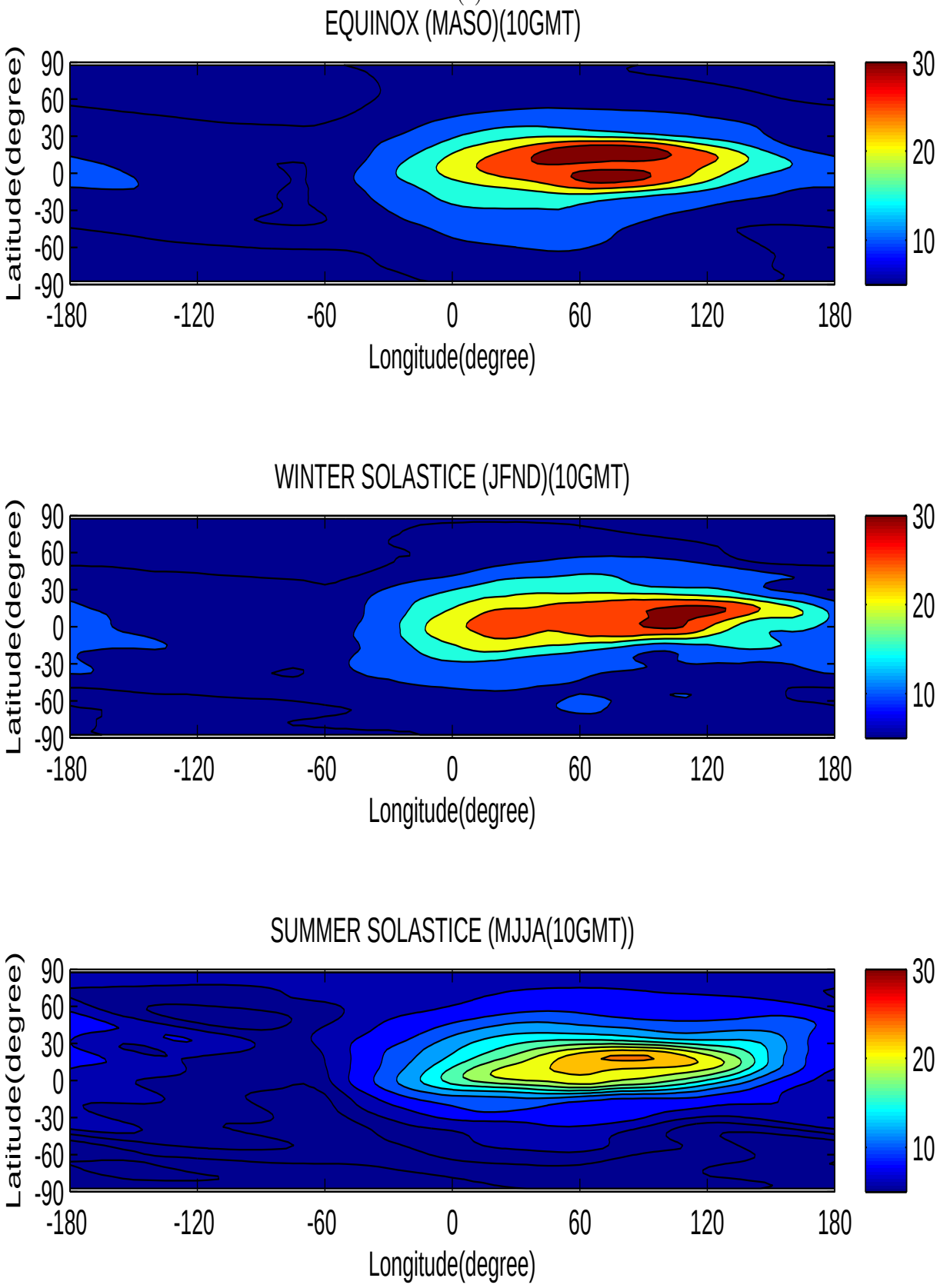
EQUINOX (MASO)(10GMT)
Latitude(degree)
90
60
30
0
-30
-60
-90
-180
-120
-60
0
60
120
180
Longitude(degree)
30
20
10
WINTER SOLASTICE (JFND)(10GMT)
Latitude(degree)
90
60
30
0
-30
-60
-90
-180
-120
-60
0
60
120
180
Longitude(degree)
30
20
10
SUMMER SOLASTICE (MJJA(10GMT))
Latitude(degree)
90
60
30
0
-30
-60
-90
-180
-120
-60
0
60
120
180
Longitude(degree)
30
20
10

(g)

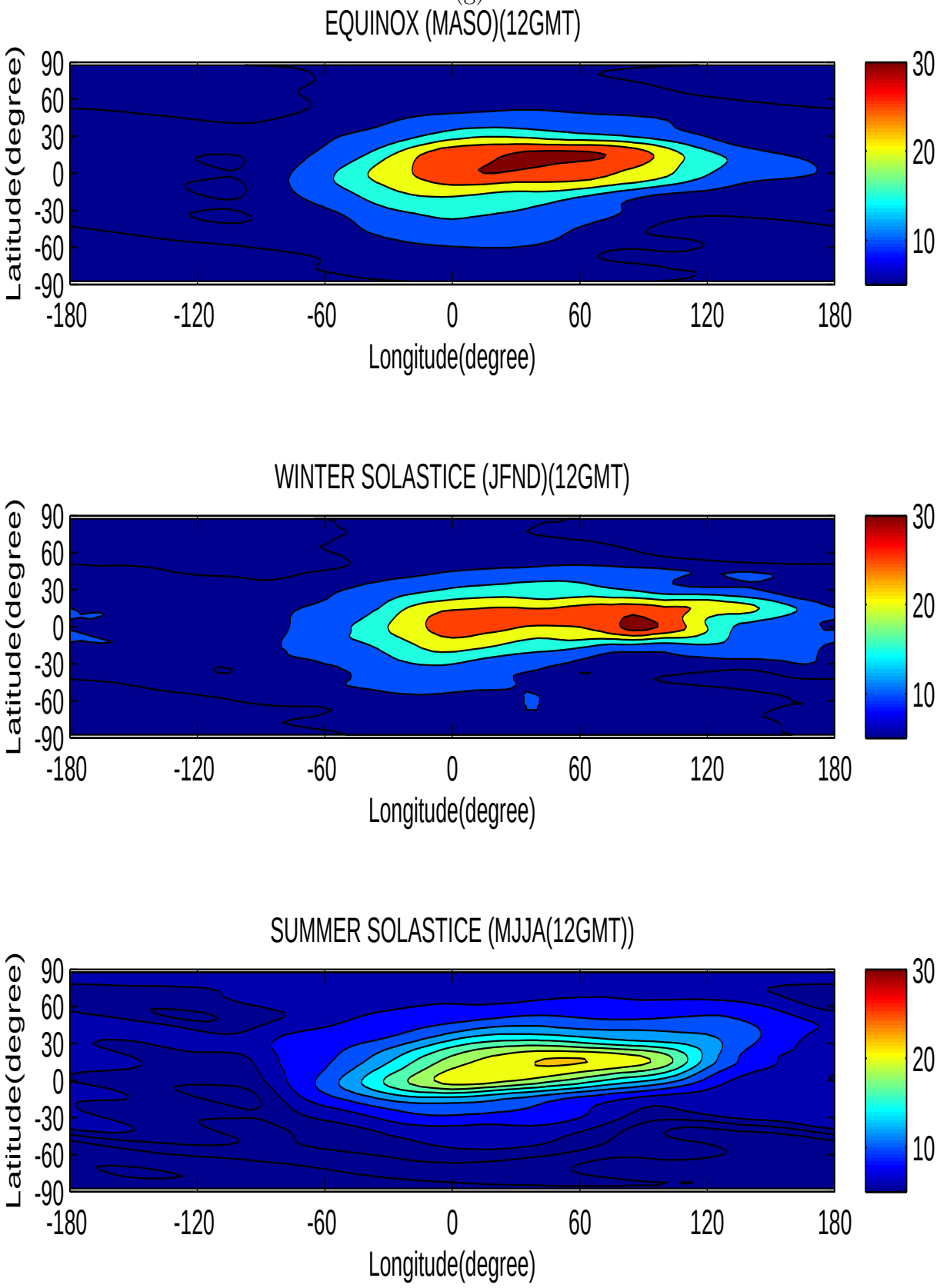
EQUINOX (MASO)(12GMT)
Latitude(degree)
90
60
30
0
-30
-60
-90
-180
-120
-60
0
60
120
180
Longitude(degree)
30
20
10
WINTER SOLASTICE (JFND)(12GMT)
Latitude(degree)
90
60
30
0
-30
-60
-90
-180
-120
-60
0
60
120
180
Longitude(degree)
30
20
10
SUMMER SOLASTICE (MJJA(12GMT))
Latitude(degree)
90
60
30
0
-30
-60
-90
-180
-120
-60
0
60
120
180
Longitude(degree)
30
20
10

(h)

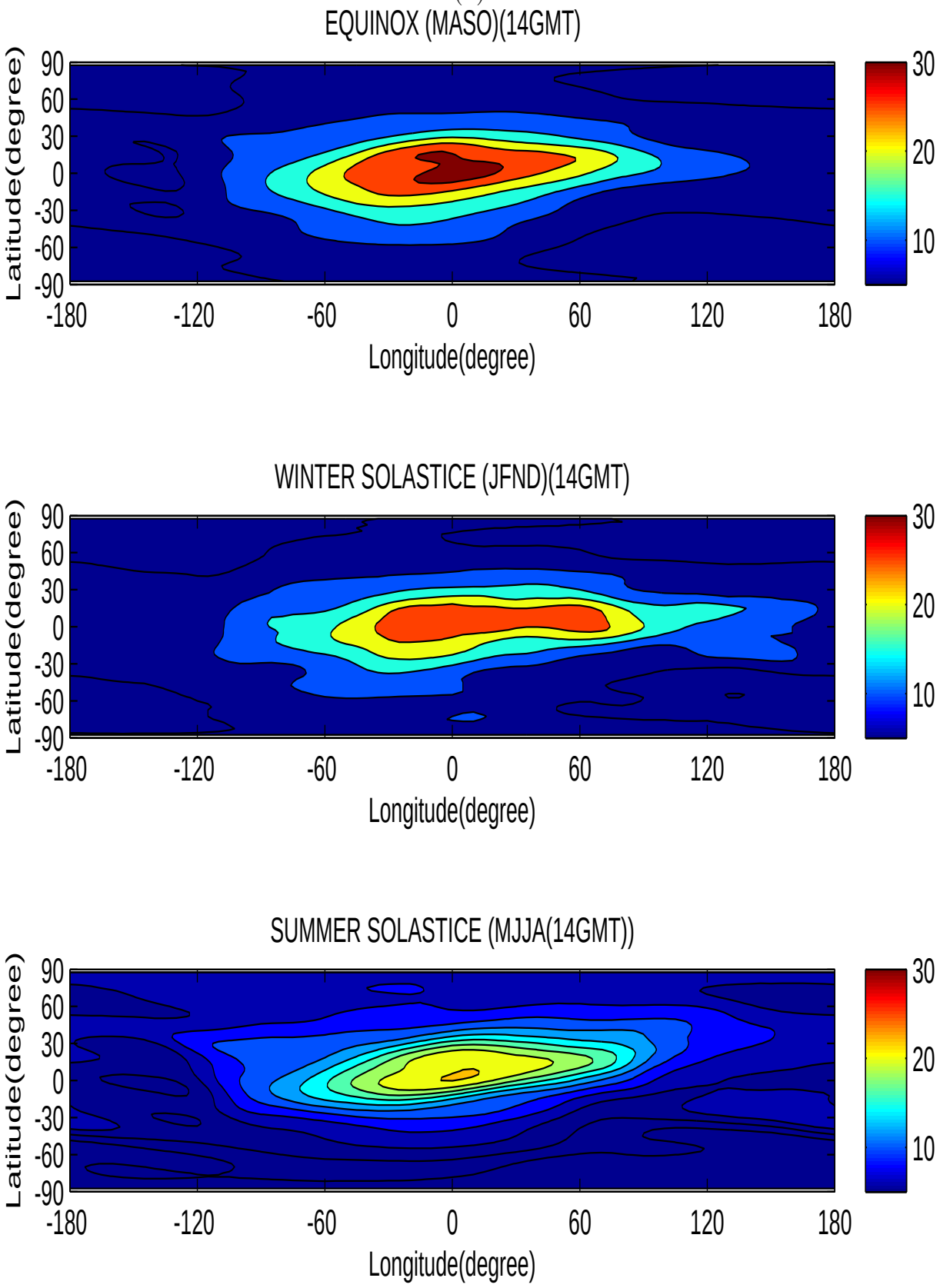
EQUINOX (MASO)(14GMT)
Latitude(degree)
90
60
30
0
-30
-60
-90
-180
-120
-60
0
60
120
180
Longitude(degree)
30
20
10
WINTER SOLASTICE (JFND)(14GMT)
Latitude(degree)
90
60
30
0
-30
-60
-90
-180
-120
-60
0
60
120
180
Longitude(degree)
30
20
10
SUMMER SOLASTICE (MJJA(14GMT))
Latitude(degree)
90
60
30
0
-30
-60
-90
-180
-120
-60
0
60
120
180
Longitude(degree)
30
20
10

(i)

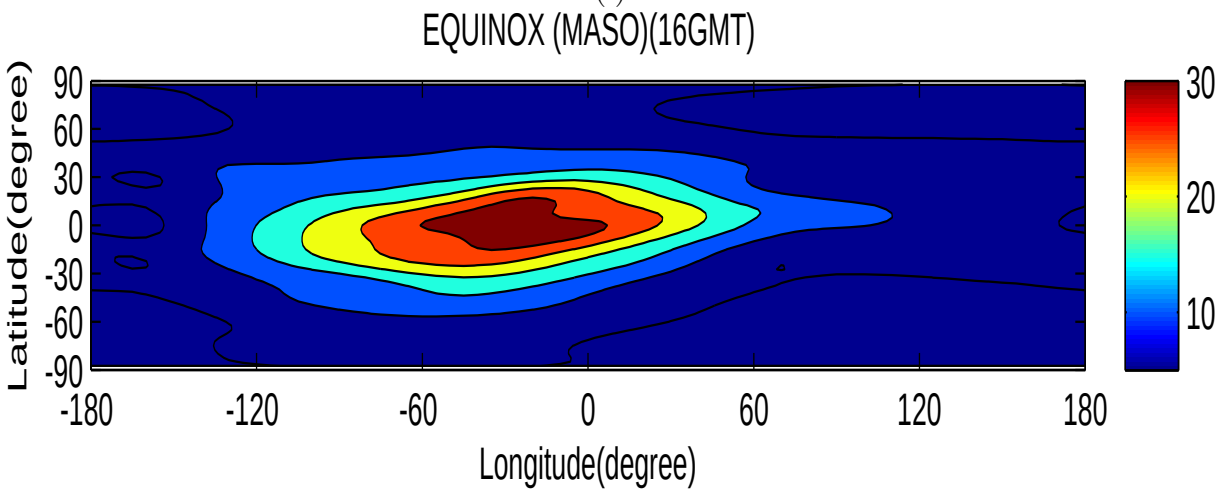
EQUINOX (MASO)(16GMT)
Latitude(degree)
90
60
30
0
-30
-60
-90
-180
-120
-60
0
60
120
180
Longitude(degree)
30
20
10

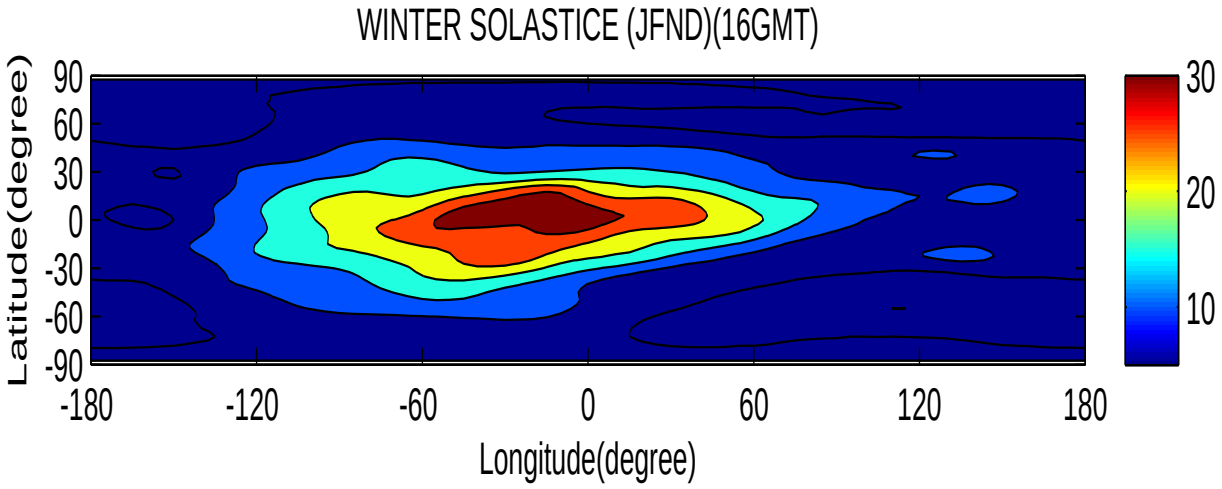
WINTER SOLASTICE (JFND)(16GMT)
Latitude(degree)
90
60
30
0
-30
-60
-90
-180
-120
-60
0
60
120
180
Longitude(degree)
30
20
10

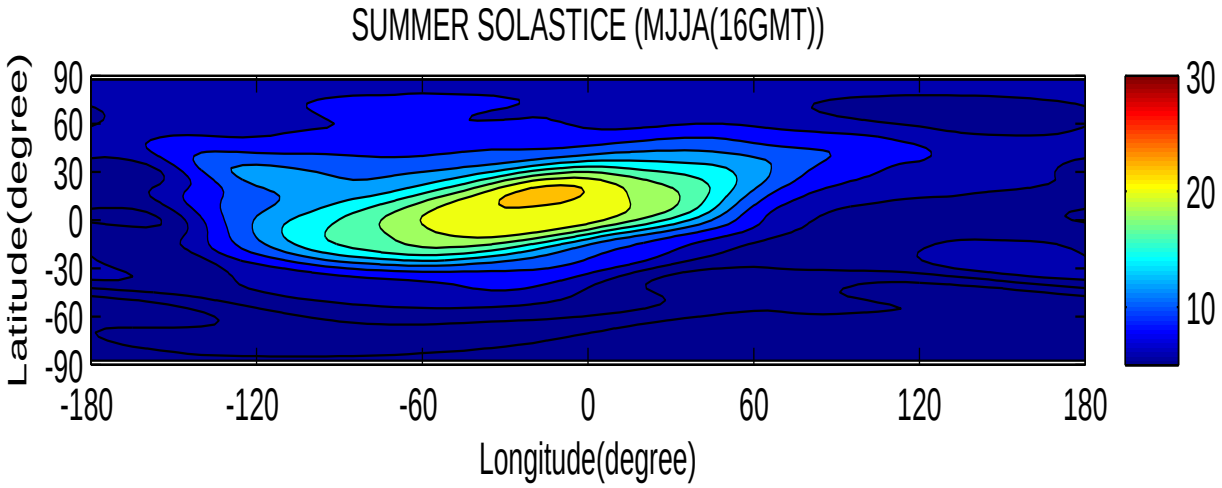
SUMMER SOLASTICE (MJJA(16GMT))
Latitude(degree)
90
60
30
0
-30
-60
-90
-180
-120
-60
0
60
120
180
Longitude(degree)
30
20
10

(j)

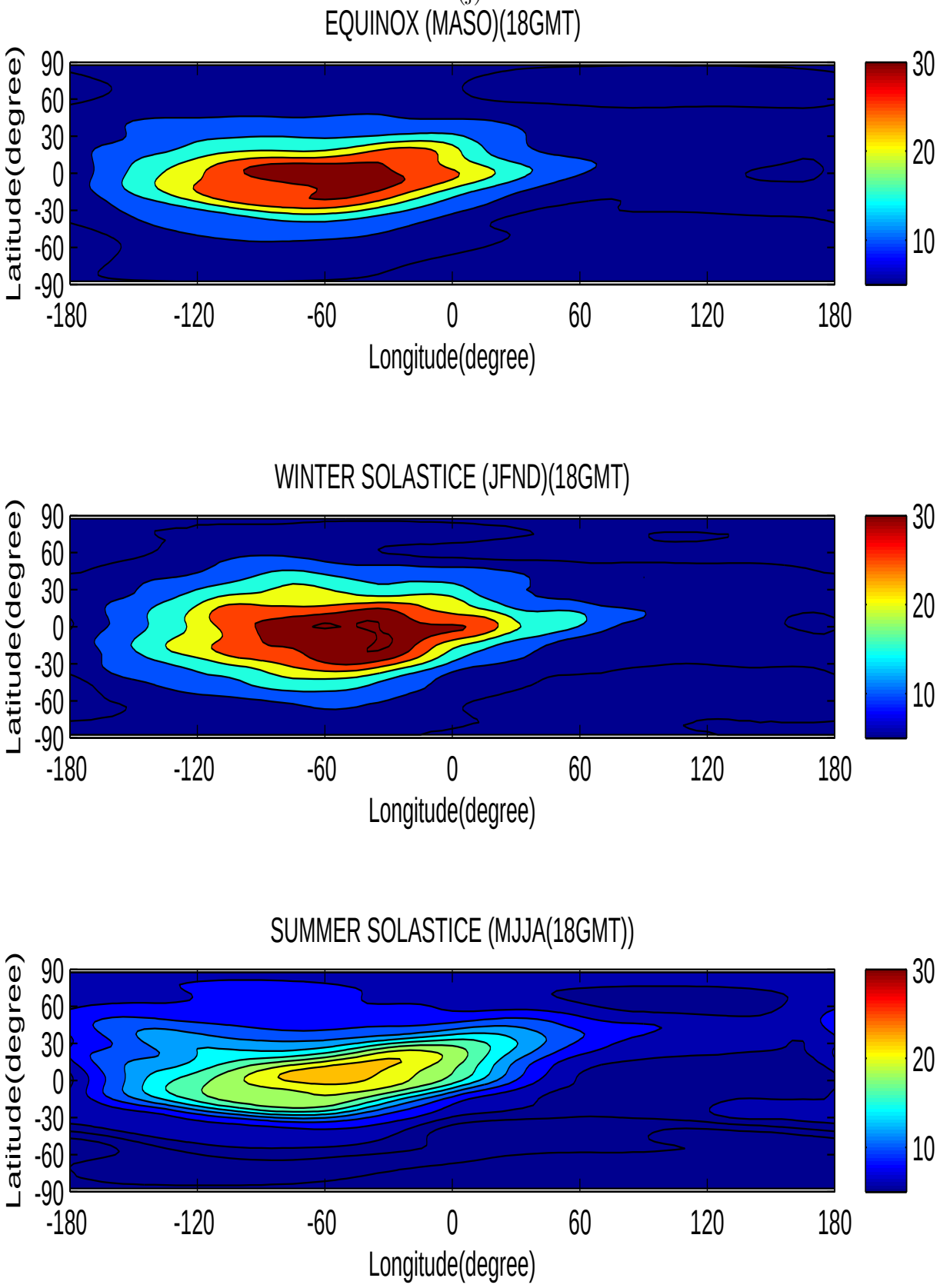
EQUINOX (MASO)(18GMT)
Latitude(degree)
90
60
30
0
-30
-60
-90
-180
-120
-60
0
60
120
180
Longitude(degree)
30
20
10
WINTER SOLASTICE (JFND)(18GMT)
Latitude(degree)
90
60
30
0
-30
-60
-90
-180
-120
-60
0
60
120
180
Longitude(degree)
30
20
10
SUMMER SOLASTICE (MJJA(18GMT))
Latitude(degree)
90
60
30
0
-30
-60
-90
-180
-120
-60
0
60
120
180
Longitude(degree)
30
20
10

(k)

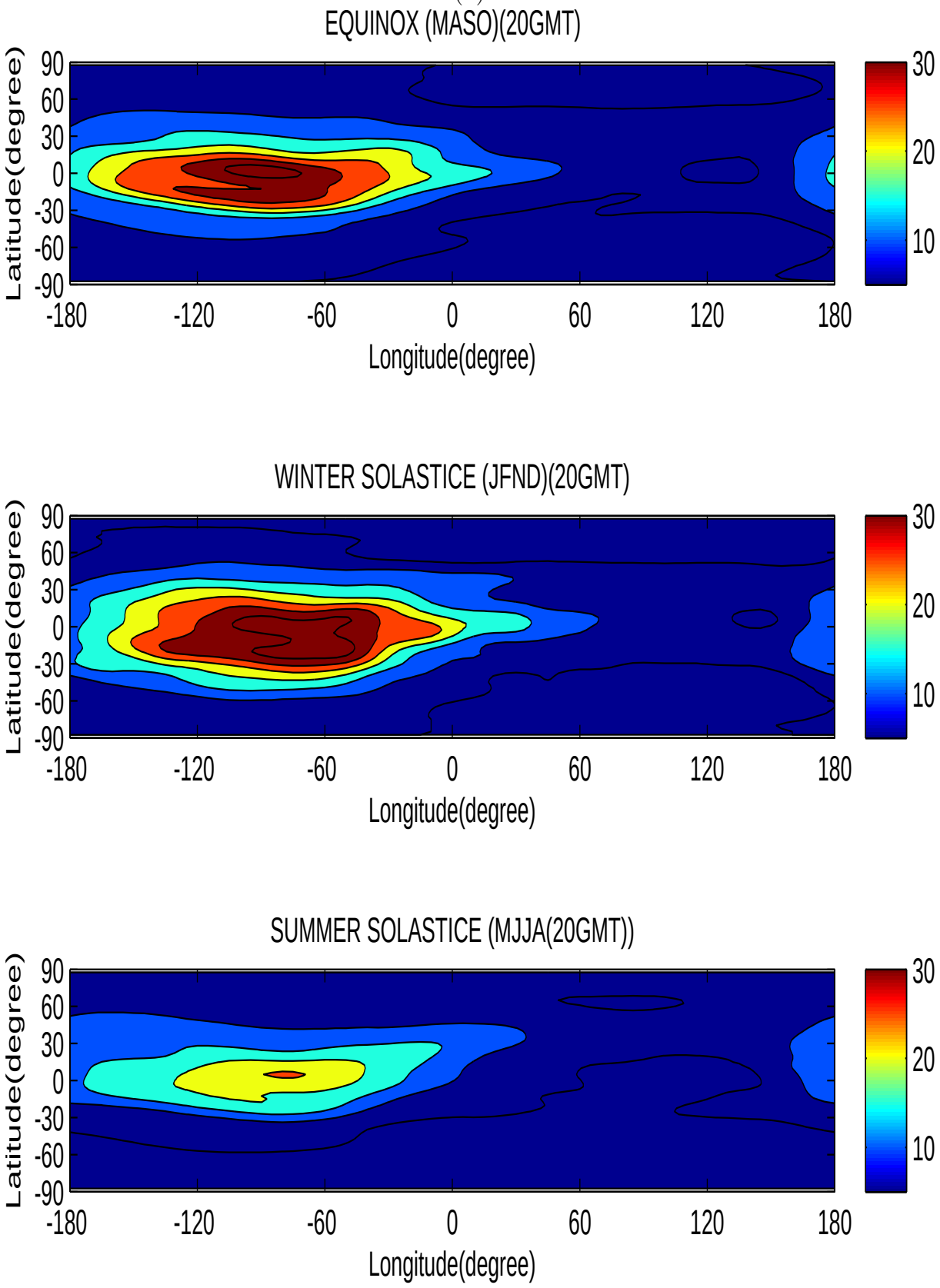
EQUINOX (MASO)(20GMT)
Latitude(degree)
90
60
30
0
-30
-60
-90
-180
-120
-60
0
60
120
180
Longitude(degree)
30
20
10
WINTER SOLASTICE (JFND)(20GMT)
Latitude(degree)
90
60
30
0
-30
-60
-90
-180
-120
-60
0
60
120
180
Longitude(degree)
30
20
10
SUMMER SOLASTICE (MJJA(20GMT))
Latitude(degree)
90
60
30
0
-30
-60
-90
-180
-120
-60
0
60
120
180
Longitude(degree)
30
20
10

(l)

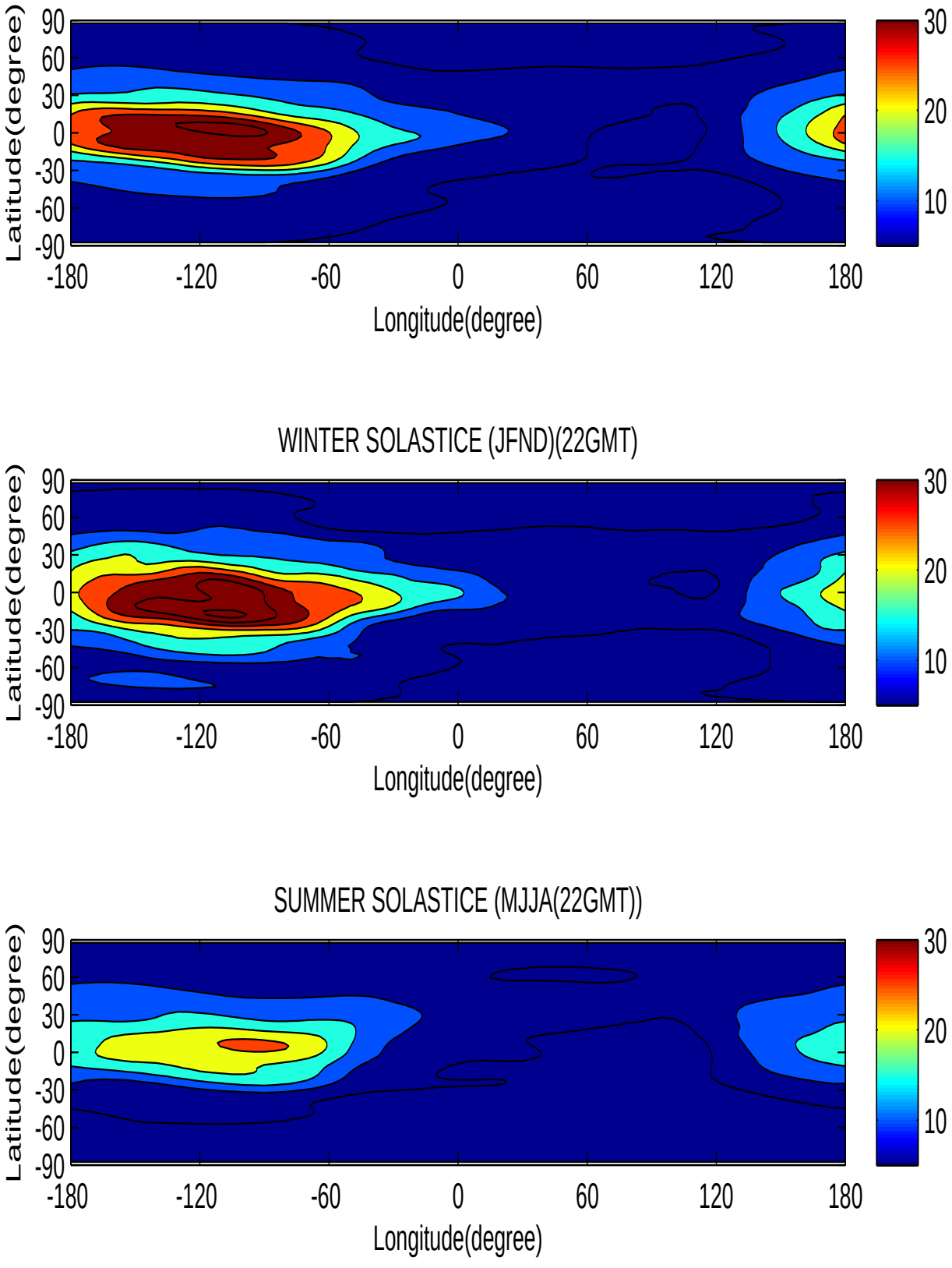

Figure 4.5: The hourly seasonal variation in TEC for the year 2008.

4.2 Seasonal variability in TEC

The seasonal variation in TEC for the 2008 has been shown in Fig 4.6. The two equinox months are combined together and summer and winter solstices are represented by groups of four months each. For example, Equinox months includes September, October, March and April, summer solstice includes the months of May, June, July and August and winter solstice is represented by November, December, January and February. As seen from the Fig. 4.6, the variation during equinox and winter are almost similar whereas the variation during summer differs markedly from the rest of the two periods. The equinoxial months show highest values of TEC. These are followed by the winter months. The lowest values of TEC are obtained in the summer months. As seen from Figs. 4.6, one can clearly see the annual or seasonal behavior of the ionosphere plasma density that deviate from the zenith angle dependence and can be classified in to winter anomaly, annual anomaly and semiannual anomaly. The winter (seasonal) anomaly often observed at mid latitudes is a phenomena during which the day time electron density of F- peak height (NmF_2) is greater in winter than summer. So our result is consistent in this regard. Our result also revels the existences of the annual anomaly also called annual asymmetry a phenomena in which NmF_2 combined from both hemispheres is greater during December solstice than during the June solstice. Comparing again equinoxes and solstice NmF_2 electron densities, the NmF_2 electron density of the Equinox periods is greater than that of the solstices and this phenomena is regarded as semiannual anomaly. Although the winter anomaly at the mid to high latitude regions mostly depend on changes in the $[O/N_2]$ ratio, the scenario at the low latitude region is the outcome of the additional equatorial electrodynamics over the region.

The hourly seasonal variation in TEC for 2008 as shown in Fig. 4.5, were plotted to show the seasonal hourly variations of TEC. There are important seasonal and long term variations in the ionosphere and therefore each season is represented by groups of four

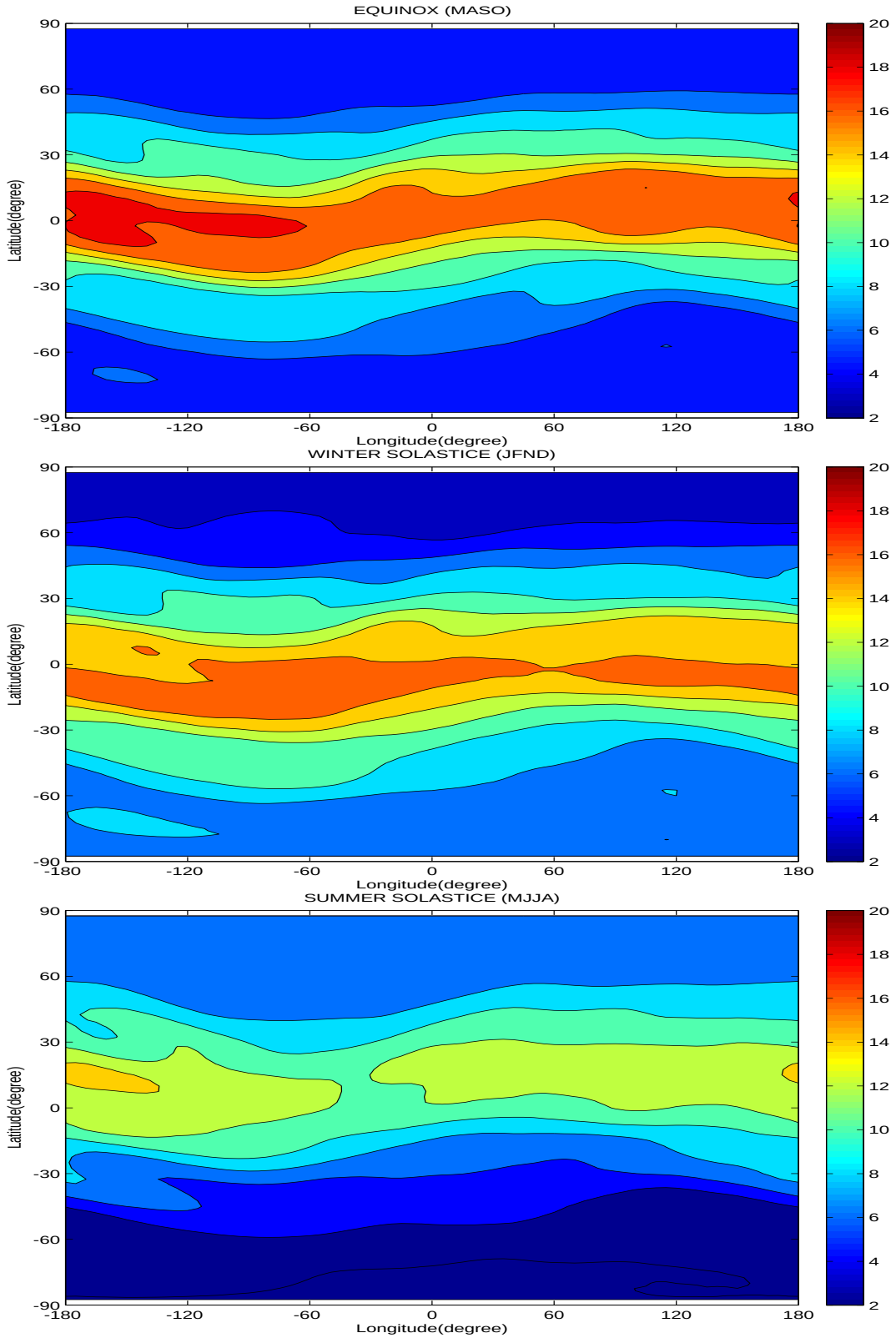

Figure 4.6: Contour plots of Seasonal variation in TEC for the year of 2008.

months in order to study these variations. During the equinoxes, the morning rise and afternoon decay of TEC is sharp compared to solstice seasons. Further, TEC is higher in the winter solstice (winter anomaly) compared to that in the summer solstice. From the Fig. 4.5, the winter solstice shows higher TEC than summer solstice. The seasonal variations of the monthly averaged values of EIA crest can be explained in terms of the composition change effect of the neutral wind [57]. Due to the unequal heating of the two hemispheres, neutral constituents are transported from the summer (hot) to the winter (cold) hemisphere. As a result, an increase of the O/N_2 ratio caused by the convection(Convection is the concerted, collective movement of groups or aggregates of molecules within fluids (e.g., liquids, gases) and rheids, either through advection or through diffusion or as a combination of both of them) of atomic oxygen is formed in the winter hemisphere as compared to summer hemisphere. Therefore, the recombination in winter hemisphere is weaker than that in the summer hemisphere, which results in the relatively higher electron concentration in winter hemisphere.

Another possible mechanism for this seasonal anomaly is the change of direction of neutral wind. A meridional component of neutral wind blows from the summer to the winter hemisphere which can reduce the crest value during summer solstice as it blows in an opposite direction to the plasma diffusion process originating from the magnetic equator; at the equinoxes, meridional winds from equator blows pole wards should result in a high ionization crest value. Based on this scenario, a seasonal effect on the crest should be expected with the crest maximum at the equinoxes and minimum in the summer.

The seasonal changes result from changes in the ratio of the concentration of atomic oxygen and molecular nitrogen in the F-region. In 2008, equinox exhibits higher TEC values compared to the summer of the same year see Fig. 4.5. This phenomena could be because of the following reasons. During the equinoxes, the sun overhead is around the equator and the temperature at the equator is hotter than at the pole therefore thermospheric meridional wind blows towards the poles from the equator. This meridional

wind changes the neutral composition and O/N_2 increase at equatorial and low latitude stations (due to stronger effect of wind transport during high solar activity). The increase will be maximum at F_2 region, and N_2 dissociation is the major process which removes ambient electrons. Hence the increase in O/N_2 ratio will result in higher electron density and therefore during equinoxes, EIA is expected to be more developed than during the solstices. This is referred to as semiannual variation. This mechanism may not work for solar minimum because of low wind effectiveness due to low ionization.

The semiannual variation of the EIA could also be due to the combined effect of the solar zenith angle and magnetic field geometry [58]. TEC diurnal peak show semiannual variation with peak during the equinox of 2008 Fig. 4.6. This implies that equinoctial semiannual variation depend largely on solar activities. It is important to mention that low solar activity that exhibited low seasonal variation, high solar activity was associated with high seasonal variation.

4.3 Latitudinal, longitudinal variations and Equatorial Ionization Anomaly (EIA)

The data has been analysed for months of year 2008, i.e. three seasons of equinox, summer and winter,respectively. The TEC variations in Fig. 4.7 shows the monthly diurnal mean of the above mentioned months. It can be seen from Fig. 4.7 that the highest values of TEC are obtained in the equinox month of March, particularly during daytime. The maximum values of TEC and maximum variations are obtained at the EIA crest, in all the twelve months. Outside of the EIA crest region, the values of TEC obtained here are found to be lower in all the months. The three typical months of year 2008, March, June and December representing three seasons of equinox, summer and winter, respectively. However, here maximum values of TEC and maximum variations are obtained at the EIA crest, i.e. $\pm 15^\circ$ latitude in all the three months. However, the diurnal peak is found to be sharper. It can be seen from Fig. 4.7 that the locations near equator and inside EIA

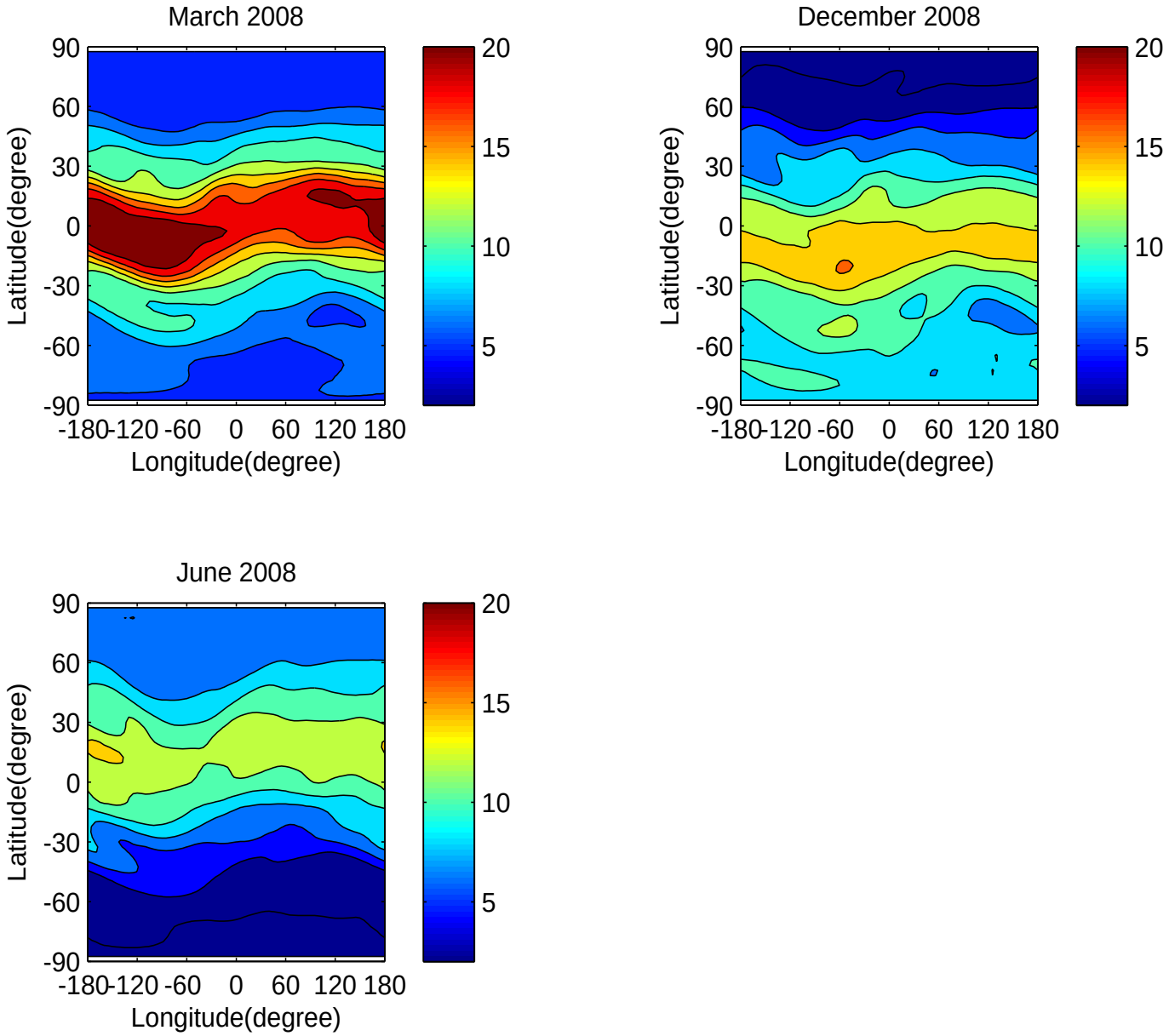

Figure 4.7: Monthly diurnal mean of TEC for the three months of: (a) March, (b) June, and (c) December.

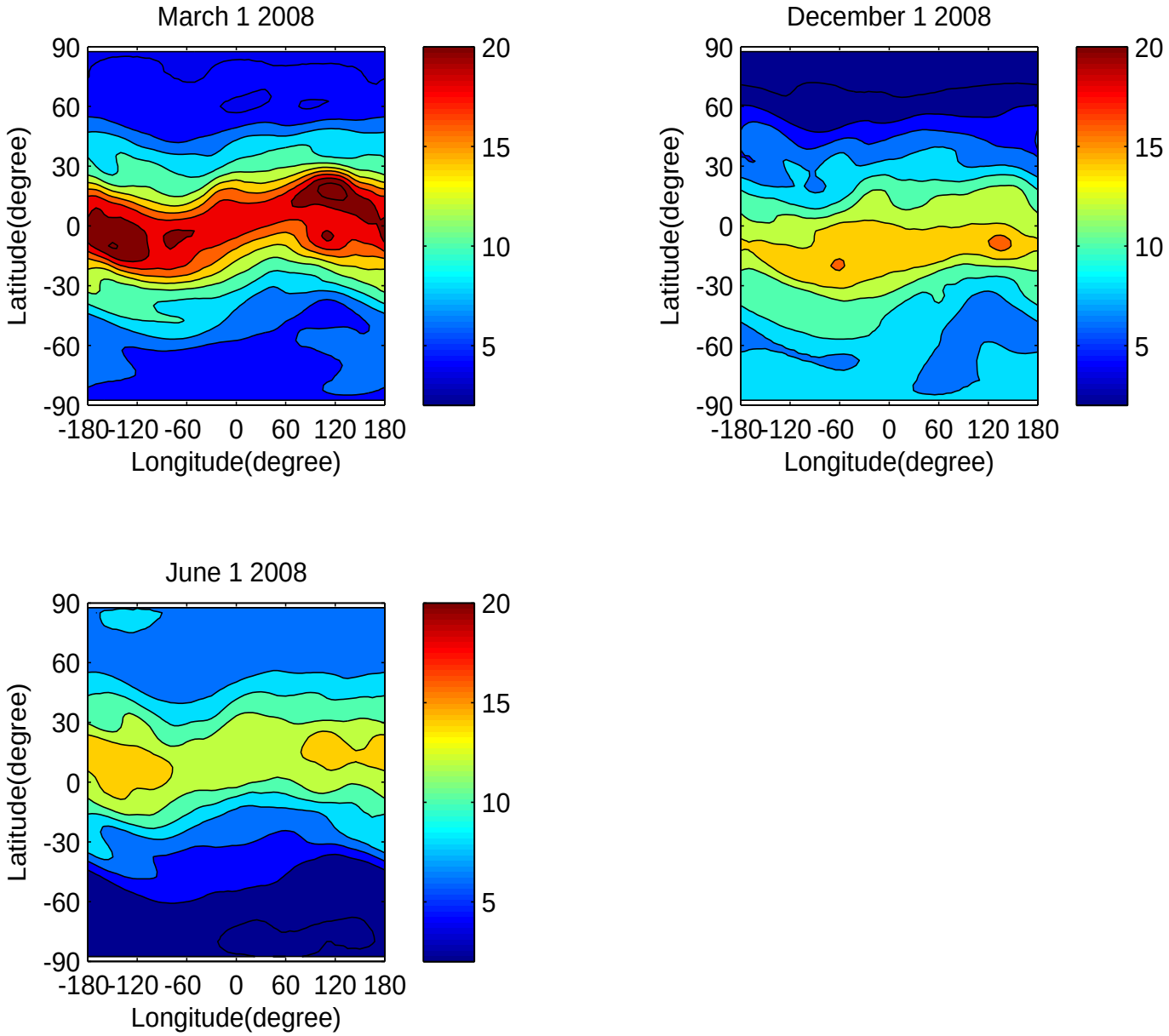

Figure 4.8: Typical TEC diurnal variations, equinoctial day (March 1, 2008), a winter day (December 1, 2008) and a summer day (Jun 1, 2008).

crest region show higher values of TEC in winter month of December in comparison to the summer month of June while the locations outside the EIA crest show lowest values in the winter month of December. This shows that, the so-called winter anomaly is seen near the equatorial and EIA crest region latitudes while it is found to be absent at low latitude outside the EIA crest during the low solar activity period considered in the study. The longitude versus latitude GMT time contour plot of TEC Figs. 4.1 and 4.5 illustrates the variation of TEC from the magnetic equator to latitudes beyond the crest of the equatorial ionization anomaly on a typical day and season. The Fig. 4.1 shows that the anomaly is non existent from 0:00 to 4:00 GMT. The anomaly builds up from around 6:00 GMT and maximizes around 14:00 GMT at $\pm 15^{\circ}$ latitudes. Thus, the major daily peak occurs around 14:00 GMT and a minor post sunset peak occurs around 18:00 GMT. The crest of the anomaly shifts equator ward as the altitude increases [59]. Therefore, the observed equator ward shift of the anomaly peak may have been caused by the fact that GPS TEC includes the plasmasphere. The plasmasphere consists of relatively cold, high density plasma that approximately corotates with the Earth.

The growth and decay of the anomaly over the year is illustrated in Figs. 4.5 and 4.6 where longitude versus latitude contours are shown for the three seasons of equinox, summer and winter, respectively. It can be seen from the Figs. 4.5, 4.6 the position, longitude, latitude span as well as the amplitude of the anomaly peak varies from month to month. In the equinoxes, the EIA crest is broader size whereas in the winter solstice, the crest of the EIA has a longer latitudinal spread. The strength of the anomaly peak also varies with season. EIA is strongest in the equinox and weakest in the summer solstice. Many earlier researchers have done work on latitudinal variations of electron density [60] have shown very good results related to the latitudinal variations of GPS TEC.

As latitude increases from the equator towards the north and south direction, the solar radiation strikes the atmosphere more obliquely. Hence, the intensity of radiation and production of free electrons decrease with increasing latitude. Near the geomagnetic

equator, the geomagnetic field is horizontal, and the electric field is eastward during the day and westward at night due to dynamic effect by atmospheric motion. This allows the region to be prone to the equatorial electro dynamic phenomena. The E region electric field is mapped into F layer through the ($E \times B$) drift of plasma which then diffuses along the slope of magnetic field lines at approximately $\pm 15^{\circ}$ geomagnetic latitudes forming crests on both the hemispheres (equatorial ionization anomaly region). Larger the plasma drift at the equator, the higher is the EEJ strength , and greater is the strength of anomaly with the crest at farther latitude from the equator. Hence, the TEC is believed to be increased gradually towards the anomaly crest regions, beyond which the value further decreases to attain lower value at mid-latitude regions. Fig. 4.8, represents the typical contour plots of TEC with its diurnal variation on an equinoctial day (March 1, 2008), a winter day (December 1, 2008), and a summer day (Jun 1, 2008). The Fig. 4.8 clearly shows gradual increase of TEC from equator to the anomaly crest beyond which it again decreases significantly. The magnitude of diurnal peak TEC is highest on the equinoctial day followed by winter day and the least value on the summer day. The latitude of crest development varies with the month, season of the year, and the solar activity condition.

Chapter 5

Conclusions and Future work

5.1 Conclusions

In this study we have used TEC observations globally distributed GPS receivers to describe the TEC variation in the ionosphere in terms of diurnal, day to day, seasonal, latitudinal and longitudinal variations during the year of 2008. In order to study the diurnal, day-to-day, seasonal, latitudinal and longitudinal TEC variations as well as to observe the EIA strength and its characteristics. We made a hourly contour plots of each month, and grouped month into seasons. The results show that the mean TEC varies from a pre dawn minimum to an afternoon maximum and then decreases. TEC variability was larger in equinox followed by winter solstice and low in summer solstice. It should be mentioned that during summer solstices, TEC diurnal values at the crest of the anomaly region exhibits lower values than TEC at the equatorial regions. This could be because sun radiation during summer solstice is not as intense as during equinox and winter therefore fountain effect is not well developed and plasma is not effectively transported off the magnetic equator. An annual seasonal variation is observed in the solstices and a semiannual variation is observed in the equinoxes. Results showed that March exhibits the larger TEC values compared to September. It can also be concluded that the ionosphere from summer to equinox responds differently (more ionization) during the August to March transition than from winter to equinox during February to September

transition (less ionization). Therefore equinox as represented by March exhibits larger TEC values. From our analysis we observed that a persistent semidiurnal variation with larger intensity during daytime was a common feature for the all events. This semidiurnal feature can be observed particularly during and after few days of the peak of the stratospheric temperature, which gives origin to an enhancement of the EIA during the morning sector, a suppression during the afternoon sector and a another enhancement during night time hours. Latitudinal study of TEC shows the clear effect of EIA crest on the TEC variations in all the seasons. During this period of study, the so called winter anomaly is seen near the equatorial and EIA crest region latitudes while it is found to be absent at low latitude outside the EIA crest.

5.2 Future work

A review of latitudinal and longitudinal profiles of TEC over glob derived from GPS IGS TEC measurements during the year of 2008 has been presented. Equatorial TEC over glob demonstrates semi-annual (equinoctial), annual (solstice), and seasonal (winter anomaly) variations with maximum values appearing during equinoctial months and minimum during solstices months. Nevertheless, the TEC above mid latitude region varies less during the day unlike the low and high latitude regions which are susceptible to the solar terrestrial disturbances. Subsequent up-gradations in the present models are applied day-by-day with sufficient number of experimental datasets and mathematical analysis for their relatively improved estimations over the equatorial and low latitude ionosphere. A near real-time TEC derivation system will also support the modeling effort of equatorial ionosphere to enhance space weather service globally.

During this period of study, the so called winter anomaly is seen near the equatorial and EIA crest region latitudes while it is found to be absent at low latitude outside the EIA crest during the low solar activity period considered in the study. However,a similar variation was been reported by Chauhan and Singh [9]. Chauhan and Singh studied

diurnaland seasonal variation of TEC at Agra in India,) there is an absence of winter anomaly at Agra station during the low solar activity period considered in the study. The other diurnal features are very similar to those obtained by earlier researchers . Future coordinated multi-instrument observations, as well as modeling studies, are essential to have a clear global understanding of such winter anomaly formation in either low solar activity or high solar activity.

Bibliography

[1] RASTOGI, R. G.AND KLOBUCHAR, J. A, 1990. Ionospheric electron content within the equatorial F2 layer anomaly belt. Journal of Geophysical Research, v. 95, n. A11, p. 19045-19052

[2] FORBES, J.M.; PALO S.E.; ZHANG X, (2000). Variability of the ionosphere, J.Atmos. Sol. Terr. Phys.,v. 62, p. 685 - 693

[3] BILITZA, D, (2000). Report from 33rd COSPAR Scientific Assembly, Warsaw, Poland, 16-23 July 2000. IRI News Lett., 7: p. 1-4.

[4] Coster, A, Komjathy A, (2008). Space weather and the global positioning system. Space Weather 6:S06D04. doi:10.1029/2008SW000400

[5] HERNANDEZ-PAJARES, M, Juan JM, Sanz J, Colombo OL, (2000). Application of ionospheric tomography to real-time GPS carrier-phase ambiguities resolution, at scales of 4001000 km and with high geomagnetic activity. Geophys Res Lett 27(13):20092012

[6] Hernndez, M, Juan JM, Sanz J, (2008). GPS data processing: code and phase Algorithms, Techniques and Recipes. *http* : $//www.gage.es/TEACHING_MATERIAL/GPS_BOOK/ENGLISH/PDGPS/BOOK_PDGPS_g$

[7] Appleton,E. V,(1946). Two Anomalies in the Ionosphere. Nature, 157:691

[8] P.K. Bhuyan, M. Chamua, P. Subrahmanyam, and S.C. Garg, (2006). Effect of solar activity on diurnal and seasonal variations of electron temperature measured by the SROSS C2 over Indian low latitudes. Advances in Space Research, 37(5):885 891.

[9] V. Chauhan, O. P. Singh, and B. Singh, (2011). Diurnal and seasonal variation of GPS-TEC during a low solar activity period as observed at a low latitude station Agra. Indian Journal of Radio and Space Physics, 40:2636.

[10] RAMA, RAO P. V. S., GOPI KRISHNA S., NIRANJAN K.;PRASAD D. S. V. V. D, (2006). Temporal and spatial variations in TEC using simultaneous measurements from the Indian GPS network ofreceivers during the solar activity period of 2004-2005, Ann. Geophys, v. 24, p. 3279-3292,

[11] BAGIYA, M. S.; JOSHI H.P.; IYER K.N.; AGGARWAL M.; RAVINDRAN S.; PATHAN B.M, (2009). TEC variations during low solar activity periods (2005-2007) near the equatorial ionospheric anomaly crest region in India, Ann Geophys (Germany), v. 27, p 1047-1057.

[12] Sridharan, R., Pallam Raju, D., and Raghavarao, R, (1994). Precursor to equatorial spread-F inOI 630.0 nm dayglow, Geophys. Res.Lett., 21, 27972800.

[13] Kumar, S. and Singh A. K, (2009). Variation of ionospheric total electron content in Indian low latitude region of the equatorial anomaly during May 2007April 2008. Adv. Space Res. 43, 155-1562.

[14] Aggarwal, M, (2011). TEC variability near northern EIA crest and comparison with IRI model. Adv. Space Res. 48, 1221-1231.

[15] Mitra, S. K, (1946). Geomagnetic control region F 2 of the ionosphere. Nature. 158, 668-669.

[16] Rishbeth and Lyon, H., Lyon, A.J., Peart, M, (1963). Diffusion in the equatorial F-layer, J. Geophys. Res. 68, 2559-2569.

[17] Martyn, D. F, (1955). Theory of height and ionization density changes at the maximum of a chmpman-like region, taking account of ion production, decay, diffusion and total drift, Proceedings Cambridge Conference, pp. 254-259, physical society, London.

[18] Duncan, R. A, (1960). The Equatorial F-region of the ionosphere. J. Atmos. Terr. Phys. 18, 89-100.

[19] Bramley, E.N., Peart, M, (1965). Effect of ionization transport on the equatorial F region. Nature 206, 1245-1246.

[20] Moffett and Hanso, R. J., Hanson, W. B, (1965). Effect of ionization transport on the equatorial F region. Nature. 206, 705-706.

[21] Heelis, R. A, (2004). Electrodynamics in the low and middle latitude ionosphere:a tutorial. J. Atmos. Solar Terr. Phys., 66, 825838.

[22] Balan, N., Bailey, G.J, (1995). Equatorial plasma fountain and its effects: possibility of an additional layer. J. Geophys. Res. 100, 21421-21432.

[23] Huang, Y.N., Cheng K., Chen, S.W, (1989). On the equatorial anomaly of the ionospheric total electron content near the northern anomaly crest region. J. Geophys. Res. 94, 13515.

[24] RISHBETH, H., AND GARRIOTT, O. K, (1969). Introduction to Ionospheric Physics, Academic, San Diego, Calif

[25] MOHANNAKUMAR, K, (2008). Stratosphere, troposphere interaction: an introduction. Cochin, India:Springer.

[26] McNamara, L. F, (1991). The ionosphere: communications, surveillance, and direction finding,Krieger.

[27] Kohl, H ; Ruster, R and Schlegel, K, (1996). Modern Ionospheric Science, European Geophysical Society.

[28] Bonnet, R. M. and Woltjer, L.: Surviving 1000 Centuries: Can We Do It?, Praxis.

[29] Giraud, A. and Petit, M, (2008). Ionospheric techniques and phenomena, Springer, 1978.

[30] Rishbeth, H., Setty, C.S.G.K, (1961, 1971). The F-layer at sunrise. J. Atmos. Terr. Phys. 20, 263. And the F region dynamo. Planet Space Sci., v. 19, p. 263.

[31] Ondoh, T. and Marubashi, K, (2001). Science of space environment, IOS Press.

[32] Ratcliffe, J. A, (1972). An introduction to the ionosphere and magnetosphere, Cambridge University Press.

[33] ABDU, M. A, (2005). Equatorial ionospherethermosphere system: electrodynamics and irregularities Advances in Space Research, v. 35, p. 771787

[34] Tascione, T.F. (1988). Introduction to Space Environment, Orbit Book Company,Malibar, Florida.

[35] RICHMOND, A.D, (1994). The ionospheric wind dynamo: effects of its coupling with different atmospheric regions. In: JOHNSON, R.M.; KILLEEN, T.L. (ed.). The upper mesosphere and lower thermosphere. Washington: American Geophysical Union.

[36] HEELIS, R.A.; P.C. KENDALL, R.J.; MOFFELT, D.W.; WINDLE and H. RISHBETH, (1974). Electrical coupling of the E and F-regions and its effects on F-region drifts and winds, Planet. Space Sci.,v. 22, p. 743-756.

[37] KELLEY, M. C, (2009). The Earth's ionosphere: plasma physics and electrodynamics. 2. ed. v.96, London: Elsevier. International Geophysics Series

[38] Sojka, J. J. and R. W, (1985). Schunk, A theoretical study of the global F-region for June Solstice, Solar Maximum and Low Magnetic Activity, Journal of Geophysical Research, vol. 90(A6), p. 5286.

[39] Ercha, A., D. Zhang, A. J. Ridley, Z. Xiao, and Y. Hao (2012), A global model:Empirical orthogonal function analysis of total electron content 19992009 data, J. Geophys. Res., 117, A03328, doi:10.1029/2011JA017238.

[40] SCHAER, S.; Markus; R. Gerhard; B. Timon, A.S., (1996). Daily Global Ionosphere Maps based on GPS Carrier Phase Data Routinely produced by the CODE Analysis Center, Proceeding of the IGS Analysis Center Workshop, Silver Spring, Maryland, pp. 181-192, USA.

[41] Ho, C. M., A. J. Mannucci, U. J. Lindqwister, X. Pi, and B. T. Tsurutani (1996), Global ionosphere perturbations monitored by the worldwide GPS network, Geophys. Res. Lett., 23, 32193222, doi:10.1029/1996GL02763

[42] Feltens and schaer, J., and S. Schaer (1998), IGS products for the ionosphere, IGS Position Paper, in IGS 1998 Analysis Center Workshop: Proceedings, edited by J. M. Dow, J. Kouba, and T. Springer, pp. 225232, EurSpace Oper. Cent., Darmstadt, Germany.

[43] Hernndez-Pajares, M., J. M. Juan, J. Sanz, R. Orus, A. Garcia-Rigo,J. Feltens, A. Komjathy, S. C. Schaer, and A. Krankowski (2009). The IGS VTEC maps: A reliable source of ionospheric information since 1998, J. Geod., 83, 263275, doi:10.1007/s00190-008-0266-1

[44] Gao, Y., P. Heroux, and J. Kouba (1994), Estimation of GPS receiver and satellite L1/L2 signal delay biases using data from CACS, paper presented at the International Symposium on Kinematic Systems in Geodesy,Geomatics, and Navigation, Univ. of Calgary, Banff, Alberta, Canada

[45] Mannucci, A. J., B. D. Wilson, D. N. Yuan, C. M. Ho, U. J. Lindqwister, and T. F. Runge (1998), A global mapping technique for GPS-derived ionospheric total electron content measurements,Radio Sci.,33, 565582.

[46] Wan, W., L. Liu, X. Pi, M.-L. Zhang, B. Ning, J. Xiong, and F. Ding (2008),Wavenumber-4 patterns of the total electron content over the low latitude ionosphere,Geophys. Res. Lett.,36, L12104, doi:10.1029/2008GL033755

[47] Rawer, K. (1984) and (1963) (Ed.), Encyclopedia of Physics, Geophysics III, Part VII,pp. 389391, Springer-Verlag, Berlin. (, in Meteorological and Astronomical Influences on Radio Wave Propagation, edited by B. Landmark, pp. 221250, Pergamon Press, Oxford.

[48] Azpilicueta, F., C. Brunini, and S. M. Radicella (2006), Global ionospheric maps from GPS observations using modip latitude, Adv. Space Res., 38, 23242331.

[49] MUELLA, M. T. A. H ; KHERANI, E. A ; DE PAULA, E. R; CERRUTI, A. P; KINTNER, P.M, KANTOR, I. J; MITCHELL, C. N; BATISTA, I. S; ABDU, M. A, (2010). Scintillationproducing Fresnelscale irregularities associated with the regions of steepest TEC gradients adjacent to the equatorial ionization anomaly. Journal of Geophysical Research , vol. 115, pp. A03301, doi:10.1029/2009JA014788.

[50] Horvath, I Essex. E.A. (2000). Using observations from the GPS and TOPEX satellites to investigate night-time TEC enhancement at mid-latitudes in the southern hemisphere during a low sunspot number period, Journal of Atmospheric and solar Terissterial-Physics, Vol .62, No.5, pp. 371-391.

[51] Klobuchar, J.A, (1987). Ionospheric time-delay algorithm for single-frequency GPS users,IEEE Transactions on aerospace and electronic systems, Vol. 23, No. 3, pp. 325-331

[52] Hansen, A.; Blanch; J Walter, (2000). Ionospheric correction analysis for WAAS quiet and stormy. ION GPS, Salt Lake City, Utah, September 19-22, 2000, pp. 634-642, America.

[53] Parkinson, B.W, (1996). GPS error anlysis, in Global Positioning System: theory and application,Vol. 1, Edited by Parkinson Spilker, American Institute of Aeronautics and Astronautics, Inc., Washington D.C., pp. 469-483.

[54] Dach, R; Hugentobler, U; Fridez, P Meindl, M, (2007). Manual of Bernese GPS Software Version 5.0, Astronomical Institute, University of Bern.

[55] Schaer, S. (1999). Mapping and Predicting the Earths Ionosphere Using the Global Positioning System, vol. 59, Geod. Geophys. Arb. Schweiz.Inst. fr Geod. und Photogramm, Zurich, Switzerland.

[56] ANDERSON, D. N., AND KLOBUCHAR J. A.,(1983). Modeling the total electron content observations above Ascension Island, J. Journal of Geophysical Research , v. 88, p. 8020-8024,

[57] BALAN, N., Otsuka, Y., and Fukao, S, (1997). New aspects in the annual variation of the ionosphere observed by the MU Radar. Geophys. Res. Lett., 24, 22872290.

[58] WU, CHIN.-CHUN; FRY, C.D; LIU, J.Y; LIOU, K; TSENG, C.L, (2004). Annual TEC variation in the equatorial anomaly region during the solar minimum: September 1996August 1997.Journal of Atmospheric and Terrestrial Physics, v. 66, p. 199207

[59] Su, Y.Z., Oyama, K.I., Bailey, G.J., Takahashi, T., Hirao, K, (1995). Comparisonof the satellite electron density and temperature measurements with plasmasphere ionosphere model. J. Geophys. Res. 100, 1459114603.

[60] Rama, Rao P V S; Gopi Krishna S; Niranjan K Prasad D S V V D, (2006). Temporal and spatial variations in TEC using simultaneous measurements from the Indian GPS network of receivers during the low solar activity period of 2004-2005, Ann Geophys (Germany), 24 pp 3279-3292.

Declaration

This thesis is my original work, has not been presented for a degree in any other University and that all the sources of material used for the thesis have been dully acknowledged.

Name: MICHEAL ELIAS

Signature:– – – – – – – – – – –

Place and time of submission: Addis Ababa University, June 2015

This thesis has been submitted for examination with my approval as University advisor.

Name: Prof. Gizaw Mengistu Tsidu

(Bostwana International University of Science and Technology/Addis Ababa University)

Signature:– – – – – – – – – ––